J. Fluid Mech. (2021), *vol*. 915, A137, doi:10.1017/jfm.2021.171

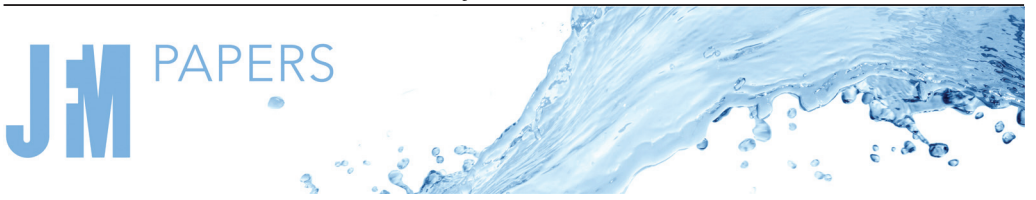

Linear stability analysis of a Newtonian ferrofluid cylinder under a magnetic field

Romain Canu[1] **and Marie-Charlotte Renoult**[1],†

[1]Normandie Univ, UNIROUEN, INSA Rouen, CNRS, CORIA, 76000 Rouen, France

(Received 16 July 2020; revised 17 February 2021; accepted 18 February 2021)

We investigate the stability of a Newtonian ferrofluid cylinder under a steady magnetic field. Linear stability analysis is performed by imposing a small-amplitude axisymmetric disturbance to the basic state. Admissible magnetic field shapes are found and dispersion relations are obtained for two general shapes: axial and non-axial. For the latter, a wire is needed to avoid a singularity at the cylinder centre. Solutions are plotted for two particular shapes previously discussed in the literature for an inviscid ferrofluid: axial and azimuthal. The applicability of the developed theory to cylinder and jet experiments using a solenoid and a wire carrying a current to create the axial and azimuthal magnetic fields, respectively, is studied. For both cases, results show that the magnetic field has a stabilising effect, as already evidenced. In addition, by solving the equation for the cutoff wavenumber, we show that, unlike the azimuthal case, the axial case cannot be stable for all wavenumbers. Taking into account the ferrofluid viscosity better explains the experimental results on ferrofluid cylinders in an azimuthal magnetic field. By choosing a specific admissible magnetic fields shape, the range of wavenumbers in which the cylinder is unstable can be controlled. A radial magnetic field is one example studied here without providing any details on the means to create the field. This latter case reveals the potential of magnetic fields to control the drop size during the ferrofluid jet breakup. These results may be of interest for applications in the printing and medical fields.

Key words: magnetic fluids, jets

1. Introduction

Magnetic liquids are used in different fields such as computer science, medicine, robotics and aeronautics with a diversity of applications such as loudspeakers, seals, brakes, dampers and measuring devices (Charles & Popplewell 1982; Charles 1987; Raj & Boulton 1987; Raj & Moskowitz 1990; Raj, Moskowitz & Casciari 1995; Scherer & Figueiredo Neto 2005). Because ferromagnetic materials in a liquid state lose their

† Email address for correspondence: renoultm@coria.fr

magnetic properties, magnetic liquids do not exist in nature and thus need to be synthesised. They comprise relatively small magnetic particles of ferromagnetic materials suspended in a carrier liquid phase (Shliomis 1974) and are not electrically conductive. Dispersants prevent the agglomeration of particles. Three kinds of magnetic fluids can be distinguished with respect to magnetic particle size and magnetic behaviour in the presence of a magnetic field (Nguyen 2012): ferrofluids, magnetorheological fluids and magnetophoretic fluids. Here, we focus on ferrofluids for which the magnetic particles measure approximately 10 nanometres in size, allowing us to consider a single liquid phase (instead of a liquid–solid two-phase system) that is water or oil based. Viscosity is independent of the magnetic field and is usually an order of magnitude greater than that of pure water. Oil-based ferrofluids are often more viscous than water-based ferrofluids, dependent on the magnetic particle concentration. The present study deals with jets of ferrofluid in magnetic fields. These jets may be capillary unstable, leading to jet breakup and drop formation, as observed in the case of non-magnetic liquid jets (e.g. the seminal work of Yarin 1993). Ferrofluid jets are used in medicine (Pankhurst *et al.* 2003) or in printing fields (Charles 1987; Abdel Fattah, Ghosh & Puri 2016; Ahmed *et al.* 2018; Löwa *et al.* 2019). In medicine, ferrofluids can be employed as contrast agents or in drug targeting with the injected drug contained in the ferrofluid jet being delivered to a specific location using a magnetic field (Lübbe *et al.* 1996; Pulfer, Ciccotto & Gallo 1999; Alexiou *et al.* 2011). In the printing domain, ferrofluids can also be employed as magnetic inks and the drops formed during the ink jet breakup are directed to a surface using a magnetic field.

For most applications, the main characteristics of capillary jet instability, namely the mean size of the drops and the time scale for their formation, need to be predicted. This can be achieved with linear stability analysis, which involves perturbing the basic flow with a small-amplitude disturbance localised in time or space. The evolution equations of the perturbation are linearised, and the solutions are searched in the form of normal modes with α the coefficient for the time variable and k the coefficient for a space variable. Solving these equations results in a dispersion relation linking the two coefficients, which determines the stable/unstable regimes. Drop formation is linked to the dominant unstable mode with the associated growth rate. The nature of the perturbation, whether spatially or temporally localised, determines the use of spatial or temporal analysis. These two approaches are illustrated for a cylindrical liquid jet in figure 1. In spatial stability analysis, k is a complex number, and α is real. The perturbation is imposed at $z = 0$ and grows along the z direction of the jet. A point on the interface moves with velocity V_{jet} in this direction. On the contrary, for temporal stability analysis, k is a real number and α is complex. In this case, the jet is represented by a doubly infinite cylinder, i.e. without any dissymmetry in the shape due to the injection. The analysis is conducted in a frame that moves with the cylinder, while a point on the interface stays at the same z location. The perturbation is imposed at time $t = 0$ along the liquid cylinder and grows over time. Keller, Rubinow & Tu (1973), and more recently Guerrero, González & García (2012) in a detailed study on all the modes of the spatial dispersion relation, showed a correspondence between these two points of view regarding the unstable solution of the dispersion relation for dimensionless jet velocities (made dimensionless with the capillary velocity) that exceeded 1. For this reason, temporal stability analysis is often used to represent liquid jets.

Several studies have conducted a temporal stability analysis of ferrofluid jets in a magnetic field while ignoring the viscosity of the ferrofluid (figure 2). In most cases, a specific magnetic field is chosen in the direction of the jet axis or in the azimuthal direction. For the axial magnetic field, Chandrasekhar (1961) studied the case of a cylindrical magnetic liquid jet in a uniform field but without specifying the method used to

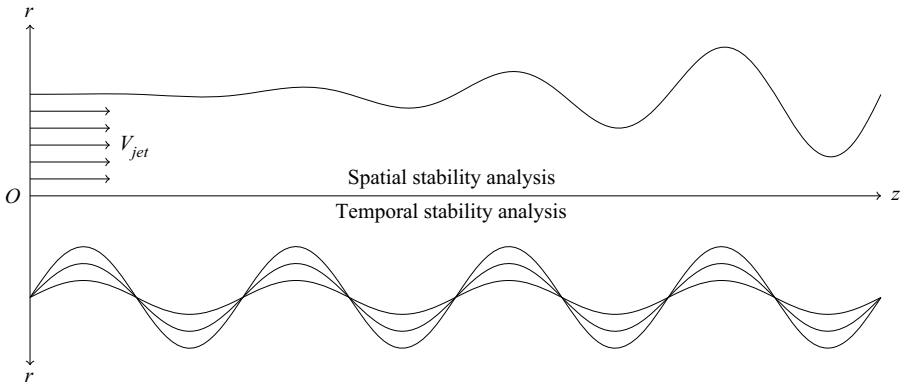

Figure 1. Representation of a cylindrical liquid jet deformed by a varicose perturbation for spatial and temporal stability analyses in the r–z plane.

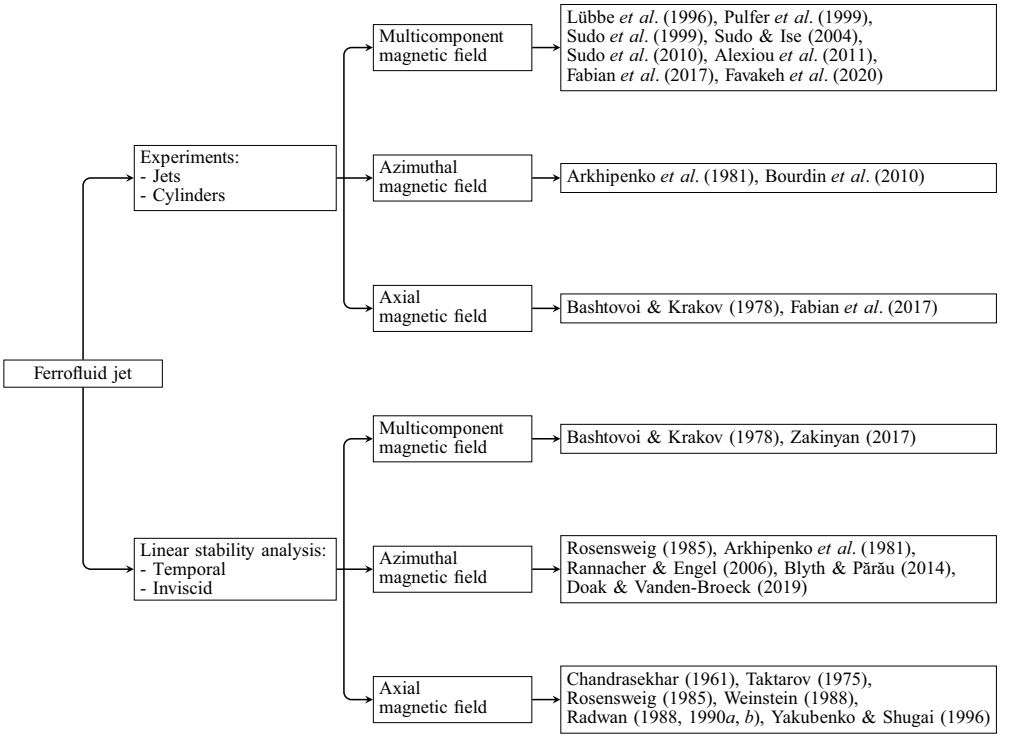

Figure 2. Studies on ferrofluid jets.

create this field. Taktarov (1975) added the presence of a solenoid as an external boundary condition, which experimentally creates an axial magnetic field. However, he assumed that its radius was much larger than the jet radius, while he did not discuss its potential effect on jet stability. Contrary to Chandrasekhar (1961), he also considered non-axisymmetric perturbations, showing that the axial magnetic field has a stabilising effect on the jet and that all non-axisymmetric perturbations are stable. Rosensweig (1985) derived this case but only for axisymmetric perturbations. Weinstein (1988) considered the effect of surrounding liquid with a different velocity than the jet. He retrieved the stabilising effect

of the axial magnetic field, although this effect was moderated by the destabilising velocity gradient between two fluids. Radwan also considered non-axisymmetric perturbations in different studies on the effect of the surrounding fluid (Radwan 1990*a*), the stability of a ferrofluid jet around gas (Radwan 1988) and the stability of a ferrofluid jet around a solid cylindrical structure (Radwan 1990*b*). He confirmed the destabilising effect of velocity gradient between two fluids, even for non-axisymmetric perturbations. He also showed a stabilising effect when the density ratio between the surrounding fluid and jet increases. Yakubenko & Shugai (1996) examined the absolute or convective aspect of instability. Experimentally, the stability of ferrofluid jet and drop formation under an axial magnetic field were respectively investigated by Bashtovoi & Krakov (1978) and Fabian *et al.* (2017); the latter used Helmholtz coils to create the field. Regarding the azimuthal field, Arkhipenko *et al.* (1981) and Rosensweig (1985) obtained the dispersion relation for a cylinder around a wire surrounded by fluid. Indeed, an azimuthal field can be generated by a wire carrying an electric current. In addition to their theoretical study, Arkhipenko *et al.* (1981) also experimentally highlighted the stabilising effect of this field with stability for all wavelengths for a sufficiently large field intensity. While exploring solitary waves on a ferrofluid jet, Blyth & Părău (2014) treated this case without considering the surrounding fluid and resolved the fully nonlinear regime of travelling solitary waves with a numerical model. In the same context, Doak & Vanden-Broeck (2019) considered a ferrofluid jet surrounded by another fluid with a solid cylindrical structure as the boundary condition. Contrary to the aforementioned studies, Rannacher & Engel (2006) studied non-axisymmetric perturbations but without finite wire thickness or an external fluid. These solitary waves were first observed by Bourdin, Bacri & Falcon (2010) on a ferrofluid cylinder subjected to an azimuthal magnetic field. Finally, Bashtovoi & Krakov (1978) and Zakinyan (2017) examined multicomponent magnetic fields with non-axisymmetric perturbations. Zakinyan (2017) considered a uniform magnetic field but, unlike the other studies, the field was non-axisymmetric. He showed that the growth rate of the perturbation depends on the angle in the azimuthal direction and that a transverse magnetic field decreases the undisturbed jet length. Experimentally, more complex magnetic fields were also applied to ferrofluid jets using coils, electromagnets or permanent magnets, to investigate the effect on drop formation (Sudo *et al.* 1999; Fabian *et al.* 2017; Favakeh, Bijarchi & Shafii 2020). An elongation of the created drops is observed in the presence of a magnetic field. Sudo & Ise (2004) and Sudo, Wakuda & Asano (2010) also studied the influence of a magnetic field on ferrofluid jets and drops. However, the jets and drops did not come from an injector but were generated using vibrations applied to a ferrofluid container.

To our knowledge, the aforementioned theoretical studies on the stability of ferrofluid jets only focus on specific applied magnetic fields with inviscid ferrofluids. As said previously, the viscosity of ferrofluids can be relatively important, which highlights the need for a theory that considers viscosity. A study on the magnetic field shape could also help control the drop formation during the ferrofluid jet breakup.

In this work, we perform a linear stability analysis of a Newtonian ferrofluid cylinder under a steady magnetic field of general shape. The bulk equations for the ferrofluid and jump conditions across the interface will be derived in a dimensionless form and linearised. The different possible shapes for the magnetic field will then be determined based on the basic state, and the linearised equations will be solved to obtain dispersion relations and equations for the cutoff wavenumber adapted to each shape. The applicability of our theory to a jet description will also be discussed. Finally, the solutions to the dispersion relation will be studied for different magnetic fields with a discussion of the experimental practicality of such configurations.

2. Formulation

We consider an incompressible Newtonian ferrofluid cylinder of infinite length under a steady axisymmetric magnetic field of general shape. The ferrofluid response to the applied magnetic field is supposed to be linear, homogeneous and isotropic. Isothermal conditions are considered, and gravity is ignored. The surrounding fluid has no velocity, with negligible density and viscosity compared to the ferrofluid. An illustration of this basic state is shown in figure 3. The notations used in this figure will be progressively introduced into this section. The basic state, subjected to magnetic field $\boldsymbol{H_0}$, is characterised by the following conditions: zero velocity in each phase; an interface position at $r = R_0$ in a cylindrical coordinate system with R_0 the radius of the ferrofluid cylinder; a constant modified pressure Π_{01} in the magnetic phase (1); and a constant pressure P_{02} in the non-magnetic phase (2); Π_{01} is related to P_{02} by a surface tension contribution of magnitude σ/R_0, with σ the surface tension, as well as by a constant magnetic contribution that will be specified below. We perturb this state by imposing a small-amplitude axisymmetric disturbance and we investigate whether the induced flow is linearly stable or unstable. The induced flow is characterised by its velocity $\boldsymbol{U_i}$ in each phase i, its modified pressure Π_i, its magnetic field $\boldsymbol{H_i}$ and the position of the interface at $r = r_s$. The vector fields are in the form $\boldsymbol{A} = (A_r, A_\theta, A_z)$, where A_r, A_θ and A_z are the radial, azimuthal and axial components of the vector, respectively. The different physical quantities are only dependent on coordinates r, z and time t due to the axisymmetry of the perturbation. The governing equations of this flow are described in the next subsections.

2.1. *Bulk equations*

The equations, valid for the ferrofluid, are first presented. The mass balance and momentum balance equations can be expressed as

$$\boldsymbol{\nabla \cdot U_1} = 0, \tag{2.1}$$

$$\rho_1 \left(\frac{\partial \boldsymbol{U_1}}{\partial t} + \boldsymbol{U_1 \cdot \nabla U_1} \right) = -\boldsymbol{\nabla} \Pi_1 + \boldsymbol{\nabla \cdot \tau_1}, \tag{2.2}$$

with ρ_1 the density, $\boldsymbol{\tau_1} = \eta_1(\boldsymbol{\nabla U_1} + \boldsymbol{\nabla U_1^t})$ the viscous stress tensor, η_1 the dynamic viscosity and Π_1 defined by $\Pi_1 = P_1 + P_s$, where P_1 refers to thermodynamic pressure and $P_s = \mu_0 \int_0^H \upsilon(\partial M_1/\partial \upsilon)\, \mathrm{d}H$ to the magnetostrictive pressure. In this last term, μ_0 is the permeability of free space, υ the specific volume and M_1 the magnetisation.

A ferrofluid is not electrically conductive by nature, so Maxwell's equations are

$$\boldsymbol{\nabla \cdot B_1} = 0, \tag{2.3}$$

$$\boldsymbol{\nabla \times H_1} = \boldsymbol{0}, \tag{2.4}$$

with $\boldsymbol{B_1}$ the magnetic induction field which can be expressed as

$$\boldsymbol{B_1} = \mu_0 (\boldsymbol{H_1} + \boldsymbol{M_1}) = \mu_1 \boldsymbol{H_1}, \tag{2.5}$$

with μ_1 the magnetic permeability of the ferrofluid, which is constant due to the linear, homogeneous and isotropic response of the medium. The equations valid for the surrounding fluid are (2.1) to (2.5) but with $\mu_2 = \mu_0$ and negligible viscosity η_2 and density ρ_2.

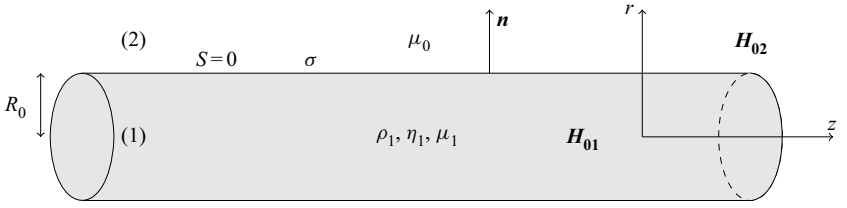

Figure 3. Representation of the basic state.

2.2. *Jump conditions across the interface*

For jump conditions across the interface, the unit normal vector is introduced. It is defined at a point on the interface, pointing from the ferrofluid to the surrounding fluid, and is given by $\boldsymbol{n} = \boldsymbol{\nabla} S/||\boldsymbol{\nabla} S|| = 1/\sqrt{1 + (\partial r_s/\partial z)^2}\boldsymbol{e_r} - (\partial r_s/\partial z)/\sqrt{1 + (\partial r_s/\partial z)^2}\boldsymbol{e_z}$, where $S = r - r_s$ is introduced to localise the position of the interface $S = 0$. The first jump condition is obtained by writing the mass balance equation at the interface without mass exchange between two phases

$$\boldsymbol{U_1} \cdot \boldsymbol{n} = -\frac{1}{||\boldsymbol{\nabla} S||}\frac{\partial S}{\partial t} \quad \text{at } r = r_s. \tag{2.6}$$

Regarding the jump conditions for momentum, there is continuity in the tangential component of stress acting on the interface

$$[(\boldsymbol{n} \cdot \boldsymbol{T}) \times \boldsymbol{n}] = \boldsymbol{0} \quad \text{at } r = r_s, \tag{2.7}$$

with the convention $[A] = A_2 - A_1$ and where $\boldsymbol{T}$ is the stress tensor such that $\boldsymbol{T_i} = -(P_i^* + (1/2)\mu_0 H_i^2)\boldsymbol{I} + \boldsymbol{B_i}\boldsymbol{H_i} + \boldsymbol{\tau_i}$, $\boldsymbol{I}$ the identity matrix, $P_i^* = \Pi_i + P_{mi}$ and $P_{mi} = \mu_0 \int_0^H M_i \, \mathrm{d}H$ the magnetic pressure. The jump of the normal component of the stress acting on the interface involves surface tension

$$[(\boldsymbol{n} \cdot \boldsymbol{T}) \cdot \boldsymbol{n}] = \sigma\kappa \quad \text{at } r = r_s, \tag{2.8}$$

with $\kappa = \boldsymbol{\nabla} \cdot \boldsymbol{n}$ the total curvature.

The jump conditions for the magnetic field imply the continuity of the normal component of $\boldsymbol{B}$ and the tangential component of $\boldsymbol{H}$ across the interface. Replacing $\boldsymbol{B}$ by expression (2.5), one finds

$$\mu_1 \boldsymbol{H_1} \cdot \boldsymbol{n} = \mu_0 \boldsymbol{H_2} \cdot \boldsymbol{n} \quad \text{at } r = r_s, \tag{2.9}$$

$$\boldsymbol{H_1} \times \boldsymbol{n} = \boldsymbol{H_2} \times \boldsymbol{n} \quad \text{at } r = r_s. \tag{2.10}$$

By using $\boldsymbol{n} \cdot \boldsymbol{I} \times \boldsymbol{n} = \boldsymbol{0}$, (2.5), (2.9) and (2.10), (2.7) and (2.8) are reduced to

$$(\boldsymbol{n} \cdot \boldsymbol{\tau_1}) \times \boldsymbol{n} = \boldsymbol{0} \quad \text{at } r = r_s, \tag{2.11}$$

$$P_1^* + P_n - (\boldsymbol{n} \cdot \boldsymbol{\tau_1}) \cdot \boldsymbol{n} = P_2 + \sigma \boldsymbol{\nabla} \cdot \boldsymbol{n} \quad \text{at } r = r_s, \tag{2.12}$$

with $P_n = (1/2)\mu_0 M_{1n}^2$; the n index referring to the normal component.

2.3. *Basic state and linearised dimensionless equations*

The bulk equations for ferrofluid (2.1) and (2.2) and the jump conditions across the interface (2.6), (2.9)–(2.12) are made dimensionless by using the Rayleigh time $\sqrt{\rho_1 R_0^3/\sigma}$,

R_0, σ/R_0, an arbitrary magnetic field intensity H_0 and μ_0 as characteristic time, length, pressure, magnetic field and magnetic permeability, respectively. The characteristic scales of the Rayleigh problem are chosen to enable the comparison of solutions with a magnetic field to those of the non-magnetic problem.

For the basic state, denoted by subscript 0 such that $\boldsymbol{H_{01}}$ is the basic state of $\boldsymbol{H_1}$ for example, the dimensionless equations become

$$\frac{\partial \Pi_{01}}{\partial r} = 0, \tag{2.13}$$

$$\frac{\partial \Pi_{01}}{\partial z} = 0, \tag{2.14}$$

$$\Pi_{01} + \tfrac{1}{2} N_{Bo,m} H_{01}^2 + \tfrac{1}{2}\left(\mu_r - 1\right) N_{Bo,m} H_{01r}^2 = P_{02} + 1 \quad \text{at } r = 1, \tag{2.15}$$

$$\mu_r H_{01r} = H_{02r} \quad \text{at } r = 1, \tag{2.16}$$

$$H_{01\theta} = H_{02\theta} \quad \text{at } r = 1, \tag{2.17}$$

$$H_{01z} = H_{02z} \quad \text{at } r = 1, \tag{2.18}$$

with $N_{Bo,m} = \mu_0(\mu_r - 1)H_0^2 R_0/\sigma$ the magnetic Bond number, and $\mu_r = \mu_1/\mu_0$ the relative permeability; $N_{Bo,m}$ can be expressed as the product of two numbers $(\mu_r - 1)$ and $\Gamma_m = \mu_0 H_0^2 R_0/\sigma$, with Γ_m a magnetic parameter that does not depend on μ_r. In (2.15), M_{01} was replaced by $(\mu_r - 1)H_{01}$ using relation (2.5) with H_{01} corresponding to the norm of the vector $\boldsymbol{H_{01}}$. From this equation, it emerges that the magnetic field has an equivalent effect on pressure jump as occurs with surface tension.

The induced flow is decomposed around the basic state, as follows: $U_i = u_i$, $\Pi_i = \Pi_{0i} + \pi_i$, $H_i = H_{0i} + h_i$ and $r_s = 1 + \zeta$ with u_i, π_i, h_i the perturbed quantities in phase i and ζ the surface perturbation. The dimensionless equations are linearised, and we thus obtain the equations for the perturbed quantities

$$\frac{1}{r}\frac{\partial r u_{1r}}{\partial r} + \frac{\partial u_{1z}}{\partial z} = 0, \tag{2.19}$$

$$\frac{\partial u_{1r}}{\partial t} + \frac{\partial \pi_1}{\partial r} - Oh\left(\frac{1}{r}\frac{\partial^2 r u_{1r}}{\partial r^2} - \frac{1}{r^2}\frac{\partial r u_{1r}}{\partial r} + \frac{\partial^2 u_{1r}}{\partial z^2}\right) = 0, \tag{2.20}$$

$$\frac{\partial u_{1z}}{\partial t} + \frac{\partial \pi_1}{\partial z} - Oh\left(\frac{1}{r}\frac{\partial r \dfrac{\partial u_{1z}}{\partial r}}{\partial r} + \frac{\partial^2 u_{1z}}{\partial z^2}\right) = 0, \tag{2.21}$$

$$u_{1r} - \frac{\partial \zeta}{\partial t} = 0 \quad \text{at } r = 1, \tag{2.22}$$

$$\frac{\partial u_{1r}}{\partial z} + \frac{\partial u_{1z}}{\partial r} = 0 \quad \text{at } r = 1, \tag{2.23}$$

$$\pi_1 + N_{Bo,m}\left(H_{01}\frac{\partial H_{01}}{\partial r}\zeta + H_{01r}h_{1r} + H_{01z}h_{1z} + (\mu_r - 1)\left(H_{01r}\frac{\partial H_{01r}}{\partial r}\zeta + H_{01r}h_{1r} - H_{01r}H_{01z}\frac{\partial \zeta}{\partial z}\right)\right) - 2Oh\frac{\partial u_{1r}}{\partial r} + \zeta + \frac{\partial^2 \zeta}{\partial z^2} = 0 \quad \text{at } r = 1, \tag{2.24}$$

$$h_{2r} - \mu_r h_{1r} + (\mu_r - 1)\, H_{01z} \frac{\partial \zeta}{\partial z} = 0 \quad \text{at } r = 1, \tag{2.25}$$

$$h_{1\theta} - h_{2\theta} = 0 \quad \text{at } r = 1, \tag{2.26}$$

$$h_{2z} - h_{1z} + (\mu_r - 1)\, H_{01r} \frac{\partial \zeta}{\partial z} = 0 \quad \text{at } r = 1, \tag{2.27}$$

with $Oh = \eta_1/\sqrt{\rho_1 \sigma R_0}$ the Ohnesorge number. The last three equations were simplified using (2.16)–(2.18).

In these equations, the magnetic field interferes with the hydrodynamic problem in the pressure term and the pressure jump across the interface.

The system of equations is linear with respect to t and z, and nonlinear with respect to r. Hence, we seek solutions in the form $A(r)\exp(\mathrm{i}kz + \alpha t)$, where $A(r)$ is an unknown function of r. Since this study explores temporal stability, we take k to be real, and $\alpha = \alpha_r + \mathrm{i}\alpha_i$ to be complex, such that k, α_r and α_i are respectively the wavenumber, growth rate and oscillation frequency of the perturbation.

3. Solution

In this section, we first determine the admissible magnetic field shapes. Then, a dispersion relation and a cutoff wavenumber equation adapted to each shape are derived.

3.1. *Admissible magnetic fields*

Based on the assumptions made in this paper, the magnetic field cannot have an arbitrary shape. It is supposed to be axisymmetric and must satisfy Maxwell equations (2.3) and (2.4), which were developed after considering a steady magnetic field and fluid that is not electrically conductive. Thus, the admissible magnetic fields must satisfy

$$\frac{\partial H_{01\theta}}{\partial z} = 0, \tag{3.1}$$

$$\frac{\partial H_{01r}}{\partial z} - \frac{\partial H_{01z}}{\partial r} = 0, \tag{3.2}$$

$$H_{01\theta} + r\frac{\partial H_{01\theta}}{\partial r} = 0, \tag{3.3}$$

$$\frac{\partial H_{01r}}{\partial r} + \frac{H_{01r}}{r} + \frac{\partial H_{01z}}{\partial z} = 0. \tag{3.4}$$

From (3.1) and (3.3), the azimuthal component must be in the form $H_{01\theta} = B/r$, with B a constant. From the basic state, it is visible that the different components of $\boldsymbol{H_{01}}$ must be independent of z. Equations (2.13) and (2.14) show that Π_{01} is constant. Moreover, it can be shown that P_{02} follows the same equations and is also a constant, hence the z independence of $\boldsymbol{H_{01}}$ seen in relation (2.15). From relations (3.2) and (3.4), it follows that H_{01z} is a constant and that component H_{01r} must be in the form A/r, with A a constant. Therefore, only the shape $\boldsymbol{H_{01}} = (A/r, B/r, C)$ with C a constant is admissible.

Two cases can be distinguished: axial magnetic fields ($A = 0, B = 0, C \neq 0$) and non-axial magnetic fields ($A \neq 0$ or $B \neq 0$). For this last case, a solid cylindrical structure (which can be a hollow or solid wire) is necessary at $r = 0$ to overcome the singularity. These two cases have different boundary conditions and are thus solved separately in the following. The methodology used to solve the equations will be detailed for the axial case. For the other case, only what differs from the axial case will be specified.

3.2. *Axial magnetic fields*

3.2.1. *Dispersion relation*

To solve the linearised equations and obtain the dispersion relation, the methodology used by Renoult *et al.* (2018) for the case of a non-magnetic liquid jet is followed. Because the velocity is divergence free, it can be expressed with a Stokes streamfunction ψ in the form $u_{1r} = -(1/r)(\partial\psi_1/\partial z)$ and $u_{1z} = (1/r)(\partial\psi_1/\partial r)$. Furthermore, the magnetic field h is curl free, and thus there exists a magnetic perturbation potential ϕ for each phase such that $\boldsymbol{h_1} = -\nabla\phi_1$ and $\boldsymbol{h_2} = -\nabla\phi_2$. The equations to be solved can be written in the following form:

$$\frac{\partial \pi_1}{\partial r} = \frac{1}{r}\frac{\partial^2\psi_1}{\partial z\partial t} + \frac{Oh}{r}\left(\frac{1}{r}\frac{\partial^2\psi_1}{\partial r\partial z} - \frac{\partial^3\psi_1}{\partial r^2\partial z} - \frac{\partial^3\psi_1}{\partial z^3}\right), \tag{3.5}$$

$$\frac{\partial \pi_1}{\partial z} = -\frac{1}{r}\frac{\partial^2\psi_1}{\partial r\partial t} + \frac{Oh}{r}\left(\frac{\partial^3\psi_1}{\partial r^3} - \frac{1}{r}\frac{\partial^2\psi_1}{\partial r^2} + \frac{1}{r^2}\frac{\partial\psi_1}{\partial r} + \frac{\partial^3\psi_1}{\partial z^2\partial r}\right), \tag{3.6}$$

$$-\frac{\partial\psi_1}{\partial z} = \frac{\partial\zeta}{\partial t} \quad \text{at } r = 1, \tag{3.7}$$

$$\frac{\partial^2\psi_1}{\partial r^2} - \frac{\partial\psi_1}{\partial r} - \frac{\partial^2\psi_1}{\partial z^2} = 0 \quad \text{at } r = 1, \tag{3.8}$$

$$\pi_1 = N_{Bo,m}\frac{\partial\phi_1}{\partial z} + 2Oh\left(\frac{\partial\psi_1}{\partial z} - \frac{\partial^2\psi_1}{\partial r\partial z}\right) - \zeta - \frac{\partial^2\zeta}{\partial z^2} \quad \text{at } r = 1, \tag{3.9}$$

$$\mu_r\frac{\partial\phi_1}{\partial r} - \frac{\partial\phi_2}{\partial r} + (\mu_r - 1)\frac{\partial\zeta}{\partial z} = 0 \quad \text{at } r = 1, \tag{3.10}$$

$$\frac{\partial\phi_1}{\partial z} - \frac{\partial\phi_2}{\partial z} = 0 \quad \text{at } r = 1. \tag{3.11}$$

Differentiating (3.5) with respect to z and (3.6) with respect to r, it can be shown that

$$\left(\frac{\partial^2}{\partial r^2} - \frac{1}{r}\frac{\partial}{\partial r} + \frac{\partial^2}{\partial z^2} - \frac{1}{Oh}\frac{\partial}{\partial t}\right)\left(\frac{\partial^2}{\partial r^2} - \frac{1}{r}\frac{\partial}{\partial r} + \frac{\partial^2}{\partial z^2}\right)\psi_1 = 0. \tag{3.12}$$

The solution ψ_1 is the sum of two contributions and has the form

$$\psi_1 = r(\hat{A}I_1(kr) + \check{A}I_1(lr) + \hat{B}K_1(kr) + \check{B}K_1(lr))\exp(\mathrm{i}kz + \alpha t), \tag{3.13}$$

with I_1 and K_1 the modified Bessel functions of the first and second kinds, and $l^2 = k^2 + (\alpha/Oh)$ a modified wavenumber. The streamfunction must be finite at $r = 0$ so $\hat{B} = 0$ and $\check{B} = 0$. Furthermore, by using (3.8), we find that

$$\psi_1 = r\hat{A}\left[I_1(kr) - \frac{2k^2}{k^2 + l^2}\frac{I_1(k)}{I_1(l)}I_1(lr)\right]\exp(\mathrm{i}kz + \alpha t). \tag{3.14}$$

Integrating (3.7) in time, it follows that

$$\zeta = \mathrm{i}\frac{k}{\alpha}\hat{A}I_1(k)\left[\frac{k^2 - l^2}{k^2 + l^2}\right]\exp(\mathrm{i}kz + \alpha t). \tag{3.15}$$

The constant of integration in relation (3.15) is zero by definition of ζ. Then, π_1 is obtained by integrating (3.6) with respect to z and using (3.5) to find the constant of integration

$$\pi_1 = \mathrm{i}\alpha\hat{A}I_0(kr)\exp(\mathrm{i}kz + \alpha t). \tag{3.16}$$

The next step is to determine ϕ in each phase. With (2.3) and (2.5), we see that $\Delta\phi = 0$ in each phase leading to

$$\phi_1 = (a_1 I_0(kr) + b_1 K_0(kr)) \exp(\mathrm{i}kz + \alpha t), \tag{3.17}$$

$$\phi_2 = (a_2 I_0(kr) + b_2 K_0(kr)) \exp(\mathrm{i}kz + \alpha t). \tag{3.18}$$

The potential should be finite at $r = 0$ and there is no perturbation when r tends to infinity, so $b_1 = 0$ and $a_2 = 0$; a_1 and b_2 are determined using relations (3.10) and (3.11), thus giving

$$\phi_1 = \left[\frac{k}{\alpha}\hat{A} I_1(k)\left[\frac{k^2 - l^2}{k^2 + l^2}\right]\frac{(\mu_r - 1)\, K_0(k)}{\mu_r I_1(k) K_0(k) + I_0(k) K_1(k)}\right] I_0(kr) \exp(\mathrm{i}kz + \alpha t). \tag{3.19}$$

Finally, the dispersion relation is obtained with the jump condition (3.9)

$$\alpha^2 + 2\alpha k^2 Oh\left[1 - \frac{I_1(k)}{I_0(k)}\left(\frac{1}{k} + \frac{2kl}{l^2 + k^2}\left(\frac{I_0(l)}{I_1(l)} - \frac{1}{l}\right)\right)\right]$$
$$- k(1 - k^2 + P_{mag})\frac{I_1(k)}{I_0(k)}\frac{l^2 - k^2}{l^2 + k^2} = 0, \tag{3.20}$$

with

$$P_{mag} = -N_{Bo,m}\,(\mu_r - 1)\, k\frac{I_0(k) K_0(k)}{\mu_r I_1(k) K_0(k) + I_0(k) K_1(k)}, \tag{3.21}$$

the magnetic field contribution to the dispersion relation. This relation is a transcendental equation due to the term $I_0(l)/I_1(l)$, which depends on α. It tends towards the relation of the Newtonian case in the absence of a magnetic field, so when $N_{Bo,m} = 0$, as reported in García & González (2008) with a different representation (note that the two representations are equivalent Brenn 2017). Because the magnetic contribution P_{mag} does not depend on α, the same number of solutions as the non-magnetic case is expected. Therefore, the dispersion relation (3.20) has a trivial solution $\alpha = 0$, two capillary solutions, and an infinite number of hydrodynamic solutions using the same terminology as García & González (2008). The trivial and hydrodynamic solutions appear when viscosity is taken into account. The hydrodynamic solutions come from the fact that l is a complex number depending on α and that $I_1(l)$ has an infinite number of roots. By taking the limit $Oh \to 0$, the dispersion relation first obtained by Taktarov (1975) is found (with a typographical error in the dispersion relation where a modified Bessel function I_1 is replaced by I_0).

3.2.2. *Cutoff wavenumber*

The cutoff wavenumber k_c is the wavenumber for which α_r changes from positive to negative (or from negative to positive) values, corresponding to the transition from the unstable to stable (or from the stable to unstable) regime. To determine it, the dispersion relation is written to eliminate the trivial solution. Simplifying by α

$$\alpha + 2k^2 Oh\left[1 - \frac{I_1(k)}{I_0(k)}\left(\frac{1}{k} + \frac{2kl}{l^2 + k^2}\left(\frac{I_0(l)}{I_1(l)} - \frac{1}{l}\right)\right)\right]$$
$$- k(1 - k^2 + P_{mag})\frac{I_1(k)}{I_0(k)}\frac{1}{Oh\left(l^2 + k^2\right)} = 0. \tag{3.22}$$

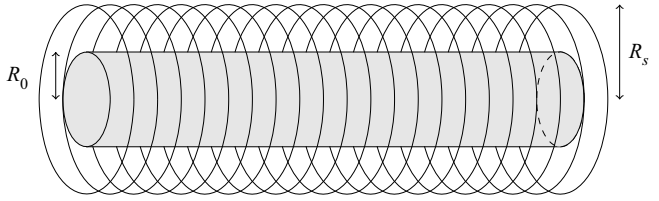

Figure 4. Representation of a ferrofluid cylinder enclosed by a solenoid.

Then, k_c corresponds to the wavenumber for which $\alpha = 0$. By taking $\alpha = 0$, we have $l^2 = k_c^2$ and relation (3.22) becomes

$$-k_c(1 - k_c^2 + P_{mag})\frac{I_1(k_c)}{I_0(k_c)}\frac{1}{2Ohk_c^2} = 0. \tag{3.23}$$

Only $(1 - k_c^2 + P_{mag})$ can be cancelled, so relation (3.23) is verified when

$$k_c^2 + k_c\frac{I_0(k_c)K_0(k_c)}{\mu_r I_1(k_c)K_0(k_c) + I_0(k_c)K_1(k_c)}(\mu_r - 1)\,N_{Bo,m} - 1 = 0. \tag{3.24}$$

From this equation, it is shown that k_c is independent of Oh.

3.2.3. *Presence of a solenoid*

Experimentally, one way to create an axial magnetic field is to use a solenoid (figure 4). It consists in a solid cylindrical structure enclosing the ferrofluid cylinder in the surrounding fluid. Therefore, the presence of a solenoid with a radius R_s leads to a supplementary boundary condition for the magnetic perturbation potential

$$\phi_2 = 0 \quad \text{at } r = \delta_s, \tag{3.25}$$

with $\delta_s = R_s/R_0$ the dimensionless solenoid radius. Thus, constant a_2 in relation (3.18) is no longer zero but is expressed as a function of b_2, leading to a new expression for ϕ_1. Only the expression of ϕ_1 (and obviously ϕ_2) is modified by the presence of the solenoid. Hence, the dispersion relation has the same form as relation (3.20) but with a different expression for P_{mag} given by

$$P_{mag} = -N_{Bo,m}\,(\mu_r - 1)\,k\frac{I_0(k)A_s}{\mu_r I_1(k)A_s + I_0(k)B_s}, \tag{3.26}$$

with $A_s = I_0(k\delta_s)K_0(k) - I_0(k)K_0(k\delta_s)$ and $B_s = I_1(k)K_0(k\delta_s) + I_0(k\delta_s)K_1(k)$.

The cutoff wavenumber for an axial magnetic field with a solenoid can also be predicted by solving the following equation:

$$k_c^2 + k_c\frac{I_0(k_c)A_s}{\mu_r I_1(k_c)A_s + I_0(k_c)B_s}(\mu_r - 1)\,N_{Bo,m} - 1 = 0, \tag{3.27}$$

derived from the cancellation of $(1 - k_c^2 + P_{mag})$. This equation tends to (3.24) for a high value of δ_s.

Figure 5. Representation of a ferrofluid cylinder with a wire.

3.3. *Non-axial magnetic fields*

3.3.1. *Dispersion relation*

For this kind of magnetic field, the constants A, B and C in $\boldsymbol{H_{01}} = (A/r, B/r, C)$ are all susceptible to having a non-zero value. Therefore, (3.9)–(3.11) have the following more general form:

$$\pi_1 = -N_{Bo,m}\left(-\left(A^2+B^2\right)\zeta - A\frac{\partial\phi_1}{\partial r} - C\frac{\partial\phi_1}{\partial z} + (\mu_r-1)\left(-A^2\zeta\right.\right.$$
$$\left.\left. -A\frac{\partial\phi_1}{\partial r} - AC\frac{\partial\zeta}{\partial z}\right)\right) + 2Oh\left(\frac{\partial\psi_1}{\partial z} - \frac{\partial^2\psi_1}{\partial r\partial z}\right) - \zeta - \frac{\partial^2\zeta}{\partial z^2} \quad \text{at } r=1, \tag{3.28}$$

$$\mu_r\frac{\partial\phi_1}{\partial r} - \frac{\partial\phi_2}{\partial r} + (\mu_r-1)\,C\frac{\partial\zeta}{\partial z} = 0 \quad \text{at } r=1, \tag{3.29}$$

$$\frac{\partial\phi_1}{\partial z} - \frac{\partial\phi_2}{\partial z} + (\mu_r-1)\,A\frac{\partial\zeta}{\partial z} = 0 \quad \text{at } r=1. \tag{3.30}$$

Then, due to the presence of a wire of radius R_w (figure 5), the dispersion relation no longer has the same form. Indeed, the singularity at $r=0$ is removed, and constants $\hat{B}$ and $\check{B}$ are no longer equal to zero in relation (3.13). Two further boundary conditions are needed: no penetration and no slip at the wire surface, which can be written into the following form

$$-\frac{1}{r}\frac{\partial\psi_1}{\partial z} = 0 \quad \text{and} \quad \frac{1}{r}\frac{\partial\psi_1}{\partial r} = 0 \quad \text{at } r=\delta_w, \tag{3.31a,b}$$

with $\delta_w = R_w/R_0$ the dimensionless wire radius. Using relation (3.31a,b) and the same methodology as in § 3.2.1, new expressions are found for ψ_1, ζ and π_1. The presence of the wire also leads to an additional boundary condition for the magnetic perturbation potential

$$\phi_1 = 0 \quad \text{at } r=\delta_w. \tag{3.32}$$

Thus, constant b_1 in relation (3.18) is no longer zero but expressed as a function of a_1, thus modifying the expression of ϕ_1. Finally, the new dispersion relation is obtained through relation (3.28)

$$\alpha^2 + 2\alpha k^2 Oh\left[1 - \frac{1}{k}\left(I_1(k) - \mathrm{d}I_1(l) - \left(\frac{cd-a}{b}\right)K_1(k) + \left(\frac{cd-a}{b}\right)\frac{K_1(k\delta_w)}{K_1(l\delta_w)}K_1(l)\right.\right.$$
$$+ d\frac{I_1(l\delta_w)}{K_1(l\delta_w)}K_1(l) - \frac{I_1(k\delta_w)}{K_1(l\delta_w)}K_1(l) + \mathrm{d}lI_0(l) + \left(\frac{cd-a}{b}\right)\frac{K_1(k\delta_w)}{K_1(l\delta_w)}K_0(l)l$$
$$\left.\left. + d\frac{I_1(l\delta_w)}{K_1(l\delta_w)}K_0(l)l - \frac{I_1(k\delta_w)}{K_1(l\delta_w)}K_0(l)l\right)\left(\frac{1}{I_0(k) + \left(\frac{cd-a}{b}\right)K_0(k)}\right)\right]$$

$$-k(1-k^2+P_{mag})\left(I_1(k)-\mathrm{d}I_1(l)-\left(\frac{cd-a}{b}\right)K_1(k)+\left(\frac{cd-a}{b}\right)\frac{K_1(k\delta_w)}{K_1(l\delta_w)}K_1(l)\right.$$
$$\left.+d\frac{I_1(l\delta_w)}{K_1(l\delta_w)}K_1(l)-\frac{I_1(k\delta_w)}{K_1(l\delta_w)}K_1(l)\right)\left(\frac{1}{I_0(k)+\left(\frac{cd-a}{b}\right)K_0(k)}\right)=0, \tag{3.33}$$

with constants a, b, c, d and the magnetic field contribution P_{mag} defined as

$$a = kI_0(k\delta_w)K_1(l\delta_w)+lI_1(k\delta_w)K_0(l\delta_w), \tag{3.34}$$
$$b = kK_0(k\delta_w)K_1(l\delta_w)-lK_1(k\delta_w)K_0(l\delta_w), \tag{3.35}$$
$$c = lI_0(l\delta_w)K_1(l\delta_w)+lI_1(l\delta_w)K_0(l\delta_w), \tag{3.36}$$
$$d=\frac{2k^2K_1(l\delta_w)\left(bI_1(k)+aK_1(k)\right)-\left(k^2+l^2\right)K_1(l)\left(bI_1(k\delta_w)+aK_1(k\delta_w)\right)}{2k^2K_1(l\delta_w)cK_1(k)-\left(k^2+l^2\right)\left(K_1(l)\left(bI_1(l\delta_w)+cK_1(k\delta_w)\right)-bI_1(l)K_1(l\delta_w)\right)}, \tag{3.37}$$
$$P_{mag}=-N_{Bo,m}\left[\mu_rA^2+B^2-\frac{(\mu_r-1)\,k\left(\mu_rA^2A_wK_1(k)-C^2B_wK_0(k)\right)}{\mu_rA_wK_0(k)+B_wK_1(k)}\right], \tag{3.38}$$

where $A_w=I_1(k)K_0(k\delta_w)+I_0(k\delta_w)K_1(k)$ and $B_w=I_0(k)K_0(k\delta_w)-I_0(k\delta_w)K_0(k)$. The dispersion relation is coherent with that obtained by Arkhipenko *et al.* (1981) in the inviscid limit without surrounding fluid (with a typographical error in the dispersion relation where the numerator and denominator were inverted, as well as the sign of one of the terms).

3.3.2. *Cutoff wavenumber*

From the dispersion relation (3.33), it is possible to obtain the equation for the cutoff wavenumber. It is not obvious *a priori* that $\alpha=0$ is a solution of relation (3.33) but it can be proved by using Taylor series. It can also be shown that the cutoff wavenumber equation is still obtained by the cancellation of $(1-k_c^2+P_{mag})$, leading to

$$k_c^2+k_c\frac{C^2B_wK_0(k_c)-\mu_rA^2A_wK_1(k_c)}{\mu_rA_wK_0(k_c)+B_wK_1(k_c)}(\mu_r-1)N_{Bo,m}-(1-N_{Bo,m}(\mu_rA^2+B^2))=0. \tag{3.39}$$

If $k_c=0$ is the solution of this equation, this means that the ferrofluid cylinder is stable for all wavenumbers (for cases where only one positive cutoff wavenumber exists). This total stability is obtained when the following condition is verified:

$$N_{Bo,m}(\mu_rA^2+B^2)-1=0. \tag{3.40}$$

3.4. *Applicability to jet description*

In this paper, we perform a temporal stability analysis of a doubly infinite liquid cylinder. We examine the applicability of this analysis to a jet description. In fact, as explained in the introduction, a spatial stability analysis is more appropriate. In this case, the solutions are searched under the form $A_s(r)\exp(\mathrm{i}(k_sz-\alpha_st))$, but this time, k_s is a

complex number and α_s a real number. Consequently, the perturbation oscillates over time and grows with distance z when k_s has a negative imaginary part. Using the same methodology as in Keller *et al.* (1973), the following dimensionless parameters are introduced: $x = k_s R_0$, $\omega = \alpha_s R_0 / V_{jet}$ and $\beta = V_{jet}\sqrt{\rho R_0/\sigma}$ with β the dimensionless jet velocity. Dimensionless solutions can be expressed in a stationary coordinate system by replacing z by $z + \beta t$, giving $A(r)\exp(\mathrm{i}(xz - (\omega - x)\beta t))$. Comparing this solution to that obtained from temporal analysis (i.e. $A(r)\exp(\mathrm{i}kz + \alpha t)$), the dispersion relation of the spatial analysis is obtained by replacing k by x and α by $-\mathrm{i}\beta(\omega - x)$ in the temporal analysis. Keller *et al.* (1973) show a correspondence between the unstable spatial and temporal solution for $\beta \gg 1$, so when the dimensionless jet velocity is relatively high.

In the following section, different cases corresponding to different magnetic field shapes will be examined. For the axial case without solid core, we search the values of β for which the unstable solution for the temporal analysis is also a solution for the spatial analysis. Contrary to the work of Guerrero *et al.* (2012), where all spatial modes are studied, we restrict here the β search to the most unstable mode. For the temporal analysis, it is characterised by $\mathrm{Re}(\alpha) = \alpha_r^*$, $\mathrm{Im}(\alpha) = 0$ and $k = k^*$. Comparing once again the form of the solutions in temporal and spatial analyses, a link can be made between k and $\mathrm{Re}(x)$, between $\mathrm{Re}(\alpha)$ and $-\beta\,\mathrm{Im}(x)$, and between $\mathrm{Im}(\alpha)$ and $\beta(\mathrm{Re}(x) - \omega)$. Therefore, in the dispersion relation of the spatial analysis, $\mathrm{Re}(x) = k^*$, $\mathrm{Im}(x) = -\alpha_r^*/\beta$ and $\omega = \mathrm{Re}(x)$. This dispersion relation becomes a function that is only dependent on β, $f(\beta) = 0$. We thus search for values of β that give $|f(\beta)| < \epsilon$, where ϵ is the set convergence criterion and does not represent the difference between the dominant modes obtained with spatial and temporal analyses. For example, applying this method to the inviscid non-magnetic case and setting $\epsilon = 10^{-4}$ leads to a difference of 0.026 %.

4. Applications

This section considers magnetic fields investigated in the literature or presenting a special interest. These magnetic fields can be written in the general form $\boldsymbol{H_{01}} = (A/r, B/r, C)$ with the appropriate choice of constants A, B and C. Only this form of magnetic field shape was previously shown to be admissible. The transcendental dispersion relations (3.20) and (3.33) are solved using the method of Luck, Zdaniuk & Cho (2015) and the transcendental cutoff wavenumber equations using a zero-search procedure. The effect of magnetic field intensity and the type of ferrofluid are characterised by varying Γ_m and μ_r. Indeed, we chose to vary Γ_m instead of $N_{Bo,m}$ in order to have a parameter independent of μ_r. Finally, the experimental applicability of the theory is studied. Previous experiments are reported in table 1 with the typical values of magnetic fields.

4.1. *Axial magnetic field*

The first studied case is a constant axial magnetic field with the form $\boldsymbol{H_{01}} = (0, 0, 1)$, which corresponds to the form $\boldsymbol{H_{01}} = (A/r, B/r, C)$ with $\{A = 0; B = 0\ ; C = 1\}$. The dispersion relation associated with this case is given by (3.20).

The growth rate and pulsation of the dispersion relation solutions are shown in figure 6 as functions of the wavenumber for different Γ_m. Recall that $N_{Bo,m}$ is defined by $N_{Bo,m} = (\mu_r - 1)\Gamma_m$. *Oh* and μ_r are set to 0.55 and 2, respectively. With this value of μ_r, $N_{Bo,m} = \Gamma_m$. The solutions obtained by García & González (2008) are determined for $\Gamma_m = 0$, namely a trivial solution $\alpha = 0$, two capillary solutions and an infinite number of hydrodynamic solutions. Only two hydrodynamic solutions are visible owing to the chosen window for the values of α. Here, Γ_m depends on σ, R_0 and H_0; H_0 is not necessarily

https://doi.org/10.1017/jfm.2021.171 Published online by Cambridge University Press

Experiments	Ferrofluids (see table 2)	Jet radius R_0 (mm)	Mean to create the magnetic field	Magnetic field shape	Field intensity H (kA m^{-1})	Bond number $N_{Bo,m}$ (–)
Arkhipenko *et al.* (1981)	Oil based FF1 and FF2	{2.1; 2.8}	Wire + current $R_w = 1$ mm $L_w = \{18; 50\}$ cm	Azimuthal	{1.705; 2.274} ($I_{max} = 30$ A)	{1.33; 1.78} (FF1)
Bourdin *et al.* (2010)	Water based FF3	[2.9; 5.0]	Wire + current $R_w = 1.5$ mm $L_w = 50$ cm	Azimuthal	[3183; 5488] ($I_{max} = 30$ A)	[8.7; 15.0]
Bashtovoi & Krakov (1978)	•	0.5	•	Axial	130	1385 (FF1)
Fabian *et al.* (2017)	Oil based FF4	0.5	Helmholtz coils $R_{coil} = 7$ cm	Axial or perpendicular	[3.98; 39.8]	[0.48; 48]
Favakeh *et al.* (2020)	Oil based EFH1	0.29	Electromagnet	Multicomponent	[23.9; 75.6]	[55; 550] ($\sigma = 0.01$ N m^{-1})
Pulfer *et al.* (1999)	• EMG-111	0.1 (estimation)	Electromagnet	•	477.5	3737 (FF1)
Sudo *et al.* (1999)	Water based W-35	0.26	Water cooled electromagnet	Perpendicular uniform	•	•
Sudo & Ise (2004)	Oil based HC-50	$\simeq$0.25 (estimation)	Permanent magnet	Multicomponent	71.6 (estimation)	115 ($\mu_r = 3$)
Sudo *et al.* (2010)	Water based W-40	•	2 Permanent magnets + 1 coil $R_{coil} = 7.5$ mm $L_{coil} = 10$ mm	Multicomponent (supposed)	310.4 (maximum value specified)	3948 (FF1 and $R_0 = 0.25$ mm)
Alexiou *et al.* (2011)	Water based FF5	0.1 (estimation)	Water cooled electromagnet	•	•	•
Lübbe *et al.* (1996)	• FF6	0.1 (estimation)	Permanent magnet	Multicomponent	[398; 637]	[2596; 6651] (FF1)

Table 1. Experimental conditions of previous experiments on ferrofluid jets and cylinders. Unknown data are represented by the symbol •. Data in brackets are used for estimations.

Name	Components	ρ (kg m^{-3})	η (kg m^{-1} s^{-1})	σ (N m^{-1})	μ_r (–)
FF1	kerosene + magnetite + oleic acid	1220	6×10^{-3}	9.2×10^{-3} (with glycerine)	2.2
FF2	kerosene + magnetite + oleic acid	1157	6×10^{-3}	1.1×10^{-2} (with glycerine)	3.5
FF3	water + maghemite	1534	1.4×10^{-3}	5.5×10^{-3} (with Freon)	1.75
FF4	•	1560	6×10^{-2}	3.24×10^{-2} (with air)	1.78
EFH1	light hydrocarbon + magnetite + oil	1210	6×10^{-3}	•	3.64
EMG-111	magnetite	•	•	•	•
W-35	water	•	•	•	•
HC-50	kerosene	1250	6×10^{-3}	2.8×10^{-2} (with air)	•
W-40	water	•	•	•	•
FF5	water + magnetite	•	•	•	•
FF6	magnetite + stabiliser	•	•	•	•

Table 2. Ferrofluid properties under standard laboratory conditions. Unknown data are represented by the symbol •.

defined as the applied magnetic field intensity even if it is the case here. If the same ferrofluid cylinder is considered (same σ and R_0), a modification of Γ_m thus implies a modification of the magnetic field intensity H_0. Thus, varying Γ_m shows the effect of H_0 on the stability of the liquid cylinder. In this figure, different behaviours can be distinguished: an unstable regime without oscillation characterised by $\alpha_r > 0$ and $\alpha_i = 0$ delimited by k_c, a stable regime without oscillation characterised by $\alpha_r < 0$ and $\alpha_i = 0$ and a stable oscillating regime characterised by $\alpha_r < 0$ and $\alpha_i \neq 0$ delimited by two wavenumbers k_1 and k_2. Increasing Γ_m induces an extension of the stable oscillating regime with a higher frequency of oscillation. It also reduces k_c and α_r in the unstable regime, hence increasing the extension of the stable regime.

The behaviour of k_c can be predicted with the help of (3.24). The solution of this equation as a function of Γ_m is represented in figure 7. The stabilisation of the cylinder when Γ_m increases is confirmed, and the cutoff wavenumbers visible in figure 6(*b*) are identified. High values of Γ_m (or $N_{Bo,m}$), like those plotted here, can be encountered experimentally as shown in table 1. However, the cylinder is never totally stable for an axial magnetic field. The zero value for k_c is an asymptotic value approached for Γ_m tending to infinity.

To examine the influence of the magnetic fluid on the solutions of the dispersion relation, μ_r is varied for a constant $\Gamma_m = 1$, and Oh is kept at 0.55 (figure 8). The same behaviour, as in varying Γ_m, is observed: reduction in k_c and α_r, and extension of the stable oscillating regime with a higher frequency of oscillation. This shows that, in this case, having ferrofluid with a higher relative magnetic permeability has the same effect as increasing the magnetic field intensity.

The influence of Oh on the dispersion relation is described in the literature for the non-magnetic cases (García & González 2008): reduction in growth rate and wavenumber for the most unstable mode when Oh increases, independence of Oh on k_c and dependence of Oh on k_1 and k_2 with a disappearance of the stable oscillating regime for a sufficiently

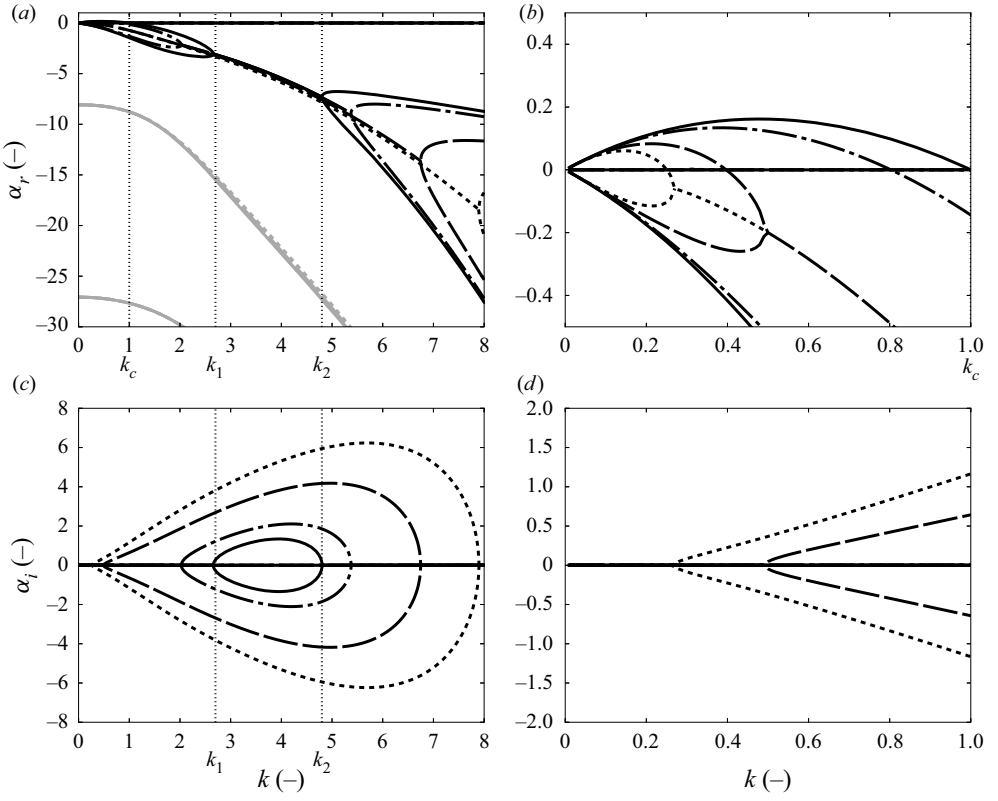

Figure 6. Solutions of the dispersion relation in an axial magnetic field for $Oh = 0.55$, $\mu_r = 2$ and different Γ_m; (*a*,*b*) α_r as a function of k, (*c*,*d*) α_i as a function of k. Panels (*b*,*d*) are blow-ups of (*a*,*c*); —— $\Gamma_m = 0$; — – – $\Gamma_m = 1$; — — $\Gamma_m = 5$; - - - - - - - - $\Gamma_m = 10$. Black lines correspond to the capillary solutions and grey lines to the hydrodynamic solutions. Vertical dotted lines represent the values of k_c, k_1 and k_2 for $\Gamma_m = 0$.

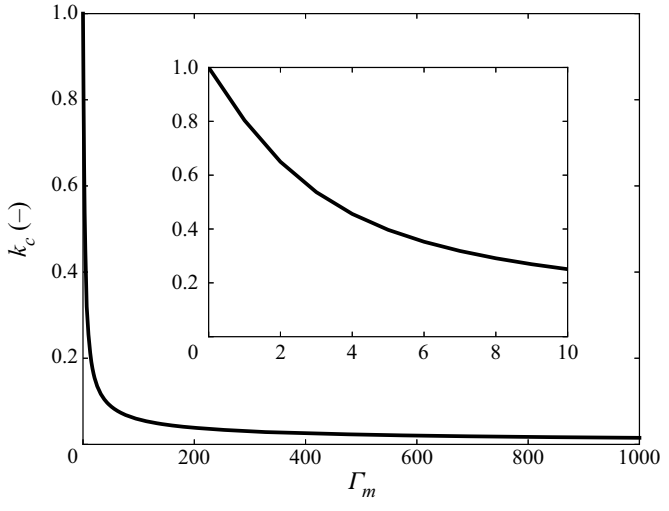

Figure 7. Value of k_c as a function of Γ_m for $\mu_r = 2$. The inset is a blow-up in the vicinity of low Γ_m.

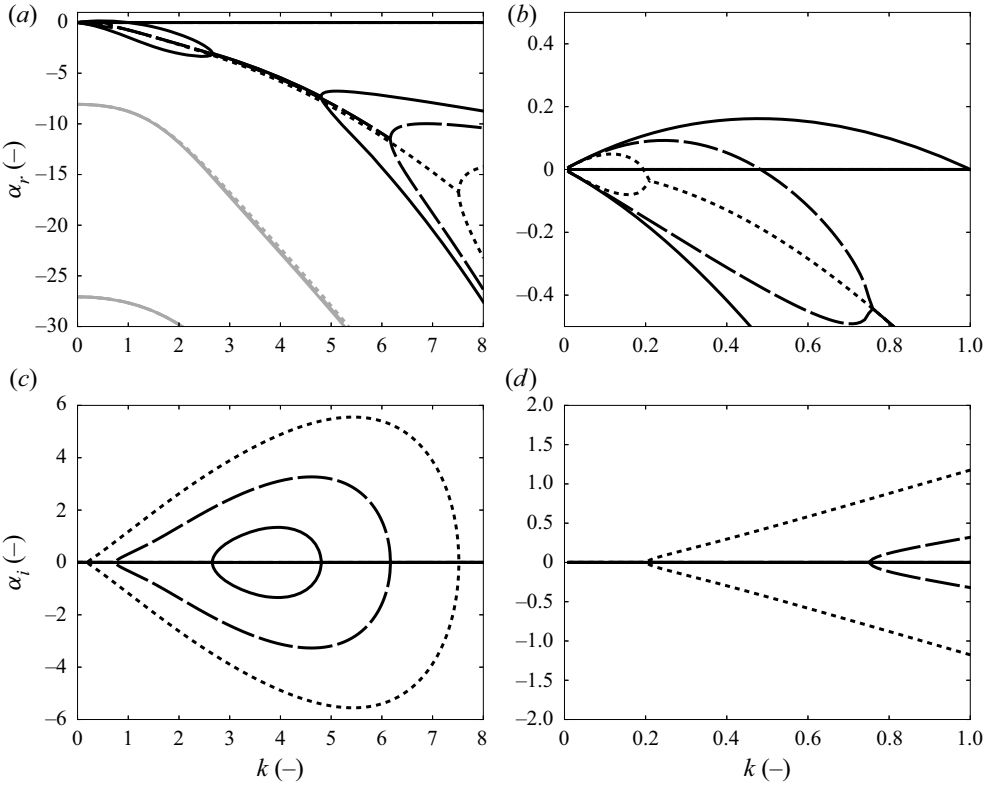

Figure 8. Solutions of the dispersion relation in an axial magnetic field for $Oh = 0.55$, $\Gamma_m = 1$ and different μ_r; (*a*,*b*) α_r as a function of k, (*c*,*d*) α_i as a function of k. Panels (*b*,*d*) are blow-ups of (*a*,*c*); —— $\mu_r = 1$; — — $\mu_r = 3$; - - - - - - - - $\mu_r = 5$. Black lines correspond to the capillary solutions and grey lines to the hydrodynamic solutions.

high value of Oh. The non-modification of k_c with respect to Oh is visible in figure 9 (dotted lines) for different values of Γ_m. However, the evolution of k_1 and k_2 as a function of Oh (solid lines) is modified with the magnetic field. As Γ_m increases, k_1 becomes increasingly independent of Oh, and for large values of Oh, k_2 varies more slowly. For lower values of Oh, the k_2 values for the different Γ_m seem to converge, as k_1 becomes closer to k_c. Moreover, the disappearance of the stable oscillating regime appears for higher values of Oh as Γ_m increases.

Experimentally, an axial magnetic field can be created using a solenoid of radius R_s and length L_s. We first assume that the length is infinite. Thus, the magnetic field created by the solenoid is

$$\boldsymbol{H} = \boldsymbol{e}_z, \tag{4.1}$$

choosing $H_0 = In$ (characteristic magnetic field used to make $\boldsymbol{H}$ dimensionless) with I the current intensity in the solenoid and n the number of turns by unit of length. This expression is a classical result, which is found in books on electromagnetism: e.g. Smythe (1950), Jackson (1962) and Pérez *et al.* (2009). The solenoid is in this case considered as a stack of N loops. In reality, the solenoid is a winding of wire; nevertheless, expression (4.1) is valid to within 1 % if the pitch of the winding does not exceed 1.35 R_s, which is often the case. The solutions for relation (3.20), with expression (3.26) for P_{mag}, are plotted in figure 10 for $Oh = 0.55$, $\mu_r = 2$, $\Gamma_m = 1$ and different values of δ_s.

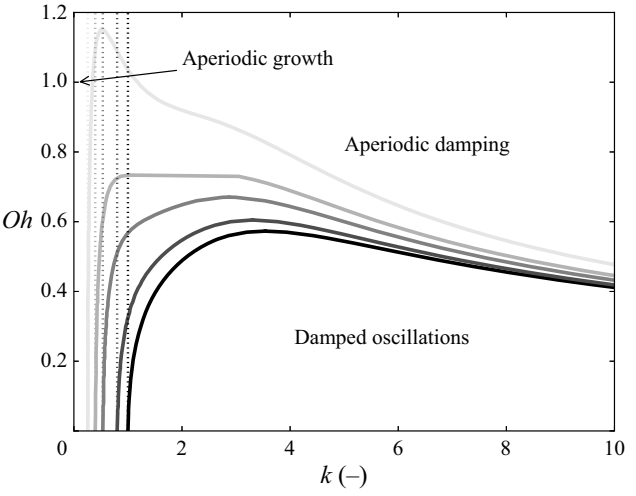

Figure 9. Delimitation of the different stability regimes for any value of k and Oh, $\mu_r = 2$ and different Γ_m. From the darkest to the lightest, $\Gamma_m = 0$, $\Gamma_m = 1$, $\Gamma_m = 3$, $\Gamma_m = 5$ and $\Gamma_m = 10$. Vertical dotted lines represent the corresponding value of k_c, and solid lines separate the regimes with and without oscillations delimited by k_1 and k_2 values.

The curves are very close to each other for different values of δ_s, and the largest offset between them is for k around the cutoff wavenumber. This can be explained by the fact that in the dispersion relation, δ_s only appears in P_{mag}, which is related to the cutoff wavenumber. A blow-up around k_c is shown in the inset, where a convergence to the solution without a solenoid is observed by increasing the value of δ_s. The curve for $\delta_s = 5$ seems to coincide with the curve which corresponds to the case without a solenoid. Consequently, for this case ($Oh = 0.55$, $\mu_r = 2$ and $\Gamma_m = 1$), we can neglect the effect of the solenoid if its radius is more than five times than that of the initial cylinder.

The cutoff wavenumber for an axial magnetic field with a solenoid is predicted by solving (3.27). Figure 10 confirms that this equation tends to (3.24) for a high value of δ_s. We thus search the value of δ_s for which the two relations converge. To do this, we can divide the numerator and denominator of the second term in (3.27) by $I_0(k\delta_s)$, giving $A_s/I_0(k\delta_s) = K_0(k) - I_0(k)K_0(k\delta_s)/I_0(k\delta_s)$ and $B_s/I_0(k\delta_s) = I_1(k)K_0(k\delta_s)/I_0(k\delta_s) + K_1(k)$. To retrieve (3.24), $A_s/I_0(k\delta_s)$ should tend to $K_0(k)$ and $B_s/I_0(k\delta_s)$ to $K_1(k)$. This leads to the two following conditions:

$$\frac{K_0(k\delta_s)}{I_0(k\delta_s)} < \epsilon \frac{K_0(k)}{I_0(k)} \quad \text{and} \quad \frac{K_0(k\delta_s)}{I_0(k\delta_s)} < \epsilon \frac{K_1(k)}{I_1(k)}, \tag{4.2a,b}$$

with ϵ a small parameter adapted according to the desired accuracy. Because $K_1(k)/I_1(k)$ is always greater than $K_0(k)/I_0(k)$, the first condition is sufficient. The value of δ_s satisfying this condition with $\epsilon = 0.01$ is shown in figure 11 as a function of the asymptotic k_c value obtained for a solenoid with an infinite radius. This figure shows that for a value $k_c = 0.8$ corresponding to $\Gamma_m = 1$, $\delta_s = 4$ is the value for which the solenoid effect can be neglected at an accuracy ϵ. This is in good agreement with $\delta_s = 5$ determined graphically in figure 10. Furthermore, we can see that for lower k_c, corresponding to greater Γ_m (figure 7), a greater value of δ_s is required, which shows that a solenoid must have a high radius when the magnetic field intensity is high. Otherwise, the effect of the presence of the solenoid cannot be neglected.

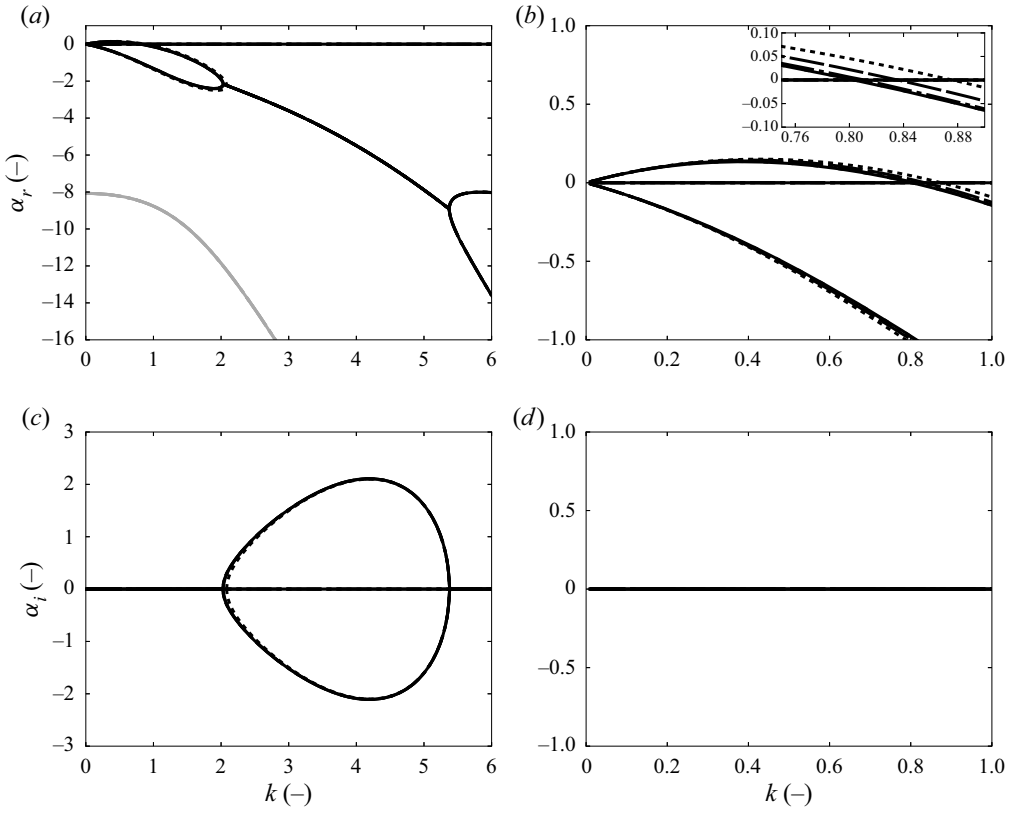

Figure 10. Solutions of the dispersion relation in an axial magnetic field created by a solenoid for $Oh = 0.55$, $\Gamma_m = 1$, $\mu_r = 2$ and different δ_s; (*a*,*b*) α_r as a function of k, (*c*,*d*) α_i as a function of k. Panels (*b*,*d*) are blow-ups of (*a*,*c*); —— no solenoid; - - - - - - - - $\delta_s = 1.5$; — — $\delta_s = 2$; — - — $\delta_s = 3$; - - - $\delta_s = 5$. Black lines correspond to the capillary solutions and grey lines to the hydrodynamic solutions. The inset is a blow-up around k_c.

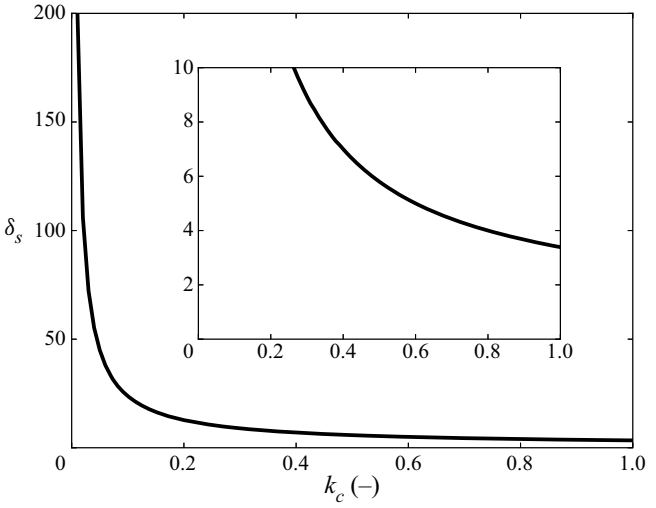

Figure 11. Value of δ_s satisfying condition (4.2*a*,*b*) as a function of k_c. The inset is a blow-up in the vicinity of small δ_s.

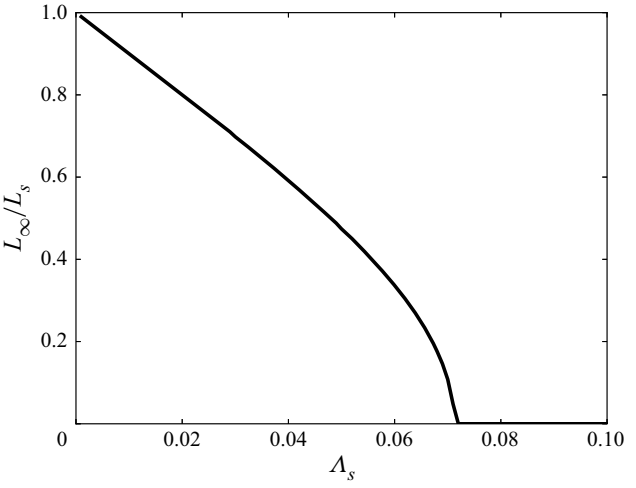

Figure 12. Portion of the solenoid where relation (4.1) is valid to within 1 % as a function of its aspect ratio Λ_s.

Until now, we have assumed that the solenoid had an infinite length. However, if it has a finite length (see for example Smythe 1950; Jackson 1962; Pérez *et al.* 2009), the magnetic field on the z axis becomes

$$\boldsymbol{H} = \frac{1}{2}\left(\frac{\dfrac{\delta_s}{2\Lambda_s}+z}{\sqrt{\delta_s^2+\left(\dfrac{\delta_s}{2\Lambda_s}+z\right)^2}}+\frac{\dfrac{\delta_s}{2\Lambda_s}-z}{\sqrt{\delta_s^2+\left(\dfrac{\delta_s}{2\Lambda_s}-z\right)^2}}\right)\boldsymbol{e_z}, \tag{4.3}$$

with $\Lambda_s = R_s/L_s$ the solenoid aspect ratio and the centre of the solenoid corresponding to the coordinate origin. Relation (4.3) tends toward relation (4.1) when the term in parentheses tends to 2. This condition is satisfied when z and δ_s are small compared to $\delta_s/2\Lambda_s$, so for a small aspect ratio Λ_s and a value of z comparable to L_s/R_0. For a given ratio δ_s and Λ_s, the range of z, L_∞, where relation (4.1) is valid within ϵ, can be determined. Taking $\epsilon = 1\,\%$, figure 12 shows that for $\Lambda_s > 0.071$, relation (4.1) is never valid. On the contrary, with $\Lambda_s = 0.02$ for example relation (4.1) is reasonable for 80 % of the length of the solenoid, showing that a small aspect ratio is necessary for using the infinite length hypothesis. In the literature, there was no experimental example combining a ferrofluid jet and a solenoid (table 1). To test the infinite length hypothesis, we rely on the characteristic scales of the coil used by Sudo *et al.* (2010). A value $\Lambda_s = 0.75$ can be calculated, and thus the infinite length hypothesis is never valid. Relation (4.3) was obtained on the z axis and the conclusions drawn previously are therefore true on this axis. Nevertheless, it was shown, e.g. by Callaghan & Maslen (1960), that relation (4.1) is accurate to within 1 % across more than 60 % of the solenoid volume for $\Lambda_s < 0.04$, which accords with the values shown in figure 12.

Finally, considering the experimental realisation of this case, as explained in § 3.4, the ferrofluid jet may be represented by a ferrofluid cylinder of infinite length if the dimensionless jet velocity β is sufficiently high. Let us determine for which β this representation is valid for the case where the radius of the solenoid is high enough to ignore the presence of the solenoid. Using the methodology explained in this subsection,

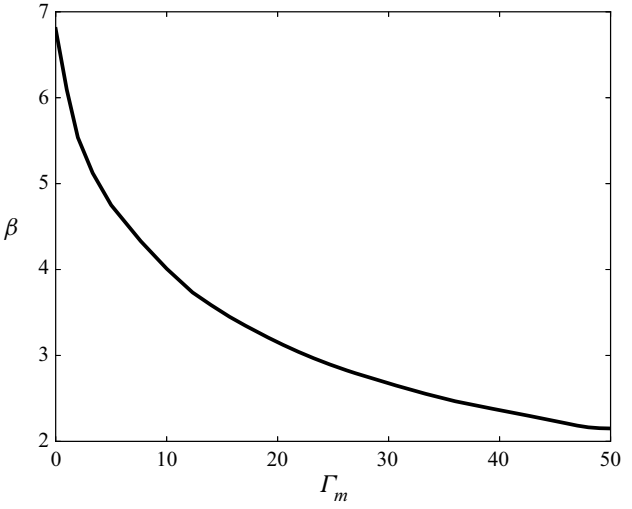

Figure 13. Minimum value of β as a function of Γ_m in an axial magnetic field for $Oh = 0.55$, $\mu_r = 2$ and $\epsilon = 10^{-4}$.

this dispersion relation can be written in the following form:

$$-\beta^2(\omega - x)^2 - 2\mathrm{i}\beta(\omega - x)x^2 Oh\left[1 - \frac{I_1(x)}{I_0(x)}\left(\frac{1}{x} + \frac{2xl'}{l'^2 + x^2}\left(\frac{I_0(l')}{I_1(l')} - \frac{1}{l'}\right)\right)\right]$$
$$- x(1 - x^2 + P_{mag})\frac{I_1(x)}{I_0(x)}\frac{l'^2 - x^2}{l'^2 + x^2} = 0, \tag{4.4}$$

with $l'^2 = x^2 - \mathrm{i}\beta(\omega - x)/Oh$. With this formalism, P_{mag} becomes

$$P_{mag} = -N_{Bo,m}(\mu_r - 1)\,x\frac{I_0(x)K_0(x)}{\mu_r I_1(x)K_0(x) + I_0(x)K_1(x)}. \tag{4.5}$$

By choosing $Oh = 0.55$, and $\mu_r = 2$ and replacing ω and x by the values mentioned in § 3.4, the minimum value of β can be found for a given Γ_m. This is the value of β so that the real and imaginary parts of relation (4.4) are less than ϵ in absolute value. Here, the value $\epsilon = 10^{-4}$ was chosen. In figure 13, the minimum value of β for considering a ferrofluid cylinder of infinite length is plotted for different values of Γ_m. To our knowledge, this value was not indicated in previous studies. We can see that a value $\beta \simeq 7$ is needed without a magnetic field and that this value decreases when the magnetic field intensity increases. Experimentally, this means that when the magnetic field intensity is strong, the jet velocity does not need to be too high in order to use a temporal stability analysis instead of spatial stability analysis. Our method for finding β was also applied to the non-magnetic case presented in the work of Guerrero *et al.* (2012) with $Oh = 0.03$ (see their figure 2) and we obtained $\beta = 29.1$. This result shows that β is dependent on Oh (since $\beta > 7$) and also that our method is consistent. Indeed, there is a difference of 13 % between their value of the dominant mode calculated with $\beta = 4.47$ and the one obtained with temporal analysis, indicating that a higher value of β is required for using temporal stability analysis.

4.2. *Azimuthal magnetic field*

We now examine an azimuthal magnetic field with the dimensionless form $\boldsymbol{H_{01}} = (0, 1/r, 0)$ corresponding to the form $\boldsymbol{H_{01}} = (A/r, B/r, C)$ with $\{A = 0; B = 1; C = 0\}$.

However, for this case, a wire is needed at the centre of the cylinder to overcome the singularity at $r = 0$. This wire is first assumed to have an infinite length. So, the dispersion relation (3.33) has to be used with $P_{mag} = -N_{Bo,m}$ by adapting expression (3.38). The cutoff wavenumber equation (3.39) is also simplified and becomes

$$k_c = \sqrt{1 - N_{Bo,m}}. \tag{4.6}$$

From this equation, it can be seen that the ferrofluid cylinder is stable for all wavenumbers when $N_{Bo,m} \geqslant 1$, which is confirmed by relation (3.40).

The total stability of the ferrofluid cylinder for $N_{Bo,m} \geqslant 1$ is visible in figure 14 where the solutions of the dispersion relation (3.33) are represented for $Oh = 0.55$, $\mu_r = 2$, $\delta_w = 0.1$ and different Γ_m. Therefore, as with the axial magnetic field, increasing the magnetic field intensity stabilises the ferrofluid cylinder. However, here the cylinder can be stable for all wavenumbers, whereas in the axial case, total stability is an asymptotic limit. The cutoff wavenumbers given by relation (4.6) are then retrieved ($k_c = 0.71$ for $\Gamma_m = 0.5$ and $k_c = 0.45$ for $\Gamma_m = 0.8$). Compared to the axial magnetic field, the hydrodynamic solutions decrease more rapidly due to their higher negative values of α_r. Two further differences should be reported. The first relates to the second capillary solution, which is no longer 0 for $k = 0$. The second concerns the stable oscillating regime characterised by two complex conjugate solutions with $\alpha_i \neq 0$. Like the axial case, increasing Γ_m increases the oscillating regime and the oscillation frequency, although this regime disappears for low values of Γ_m.

These latter observations are because of the presence of wire in the centre of the ferrofluid cylinder, as shown in figure 15, which represents the solutions of the dispersion relation (3.33) for $Oh = 0.55$, $\mu_r = 2$, $\Gamma_m = 0.5$ and different δ_w. In this figure, we can see that increasing the wire radius increases the negative values of the hydrodynamic solutions and the second capillary solution (also for $k = 0$). Increasing δ_w also decreases the maximum growth rate, with the maximum shifting towards higher wavenumber values. Furthermore, for a given magnetic field, the stable oscillating regime can be removed for a sufficiently high δ_w. The δ_w independency in the cutoff wavenumber equation (4.6) is confirmed in this figure.

Experimentally, the wire used to overcome singularity at $r = 0$ can be used to generate the azimuthal magnetic field by passing an electric current through it. When the wire is supposed to have an infinite length, the magnetic field created outside the wire is

$$\boldsymbol{H} = \frac{1}{r}\boldsymbol{e_\theta}, \tag{4.7}$$

choosing $H_0 = I/2\pi R_0$ (characteristic magnetic field used to make $\boldsymbol{H}$ dimensionless) with I the current intensity of the wire, and r the radial distance from the centre of the wire. However, if the wire has a finite length L_w (see for example Smythe 1950; Jackson 1962; Pérez *et al.* 2009), the magnetic field becomes

$$\boldsymbol{H} = \frac{1}{2r}\left(\frac{\dfrac{\delta_w}{2\Lambda_w} + z}{\sqrt{r^2 + \left(\dfrac{\delta_w}{2\Lambda_w} + z\right)^2}} + \frac{\dfrac{\delta_w}{2\Lambda_w} - z}{\sqrt{r^2 + \left(\dfrac{\delta_w}{2\Lambda_w} - z\right)^2}}\right)\boldsymbol{e_\theta}, \tag{4.8}$$

with $\Lambda_w = R_w/L_w$, the wire aspect ratio and the centre of the wire corresponding to the coordinate origin. The coefficient after $1/2r$ is the same as in expression (4.3) for

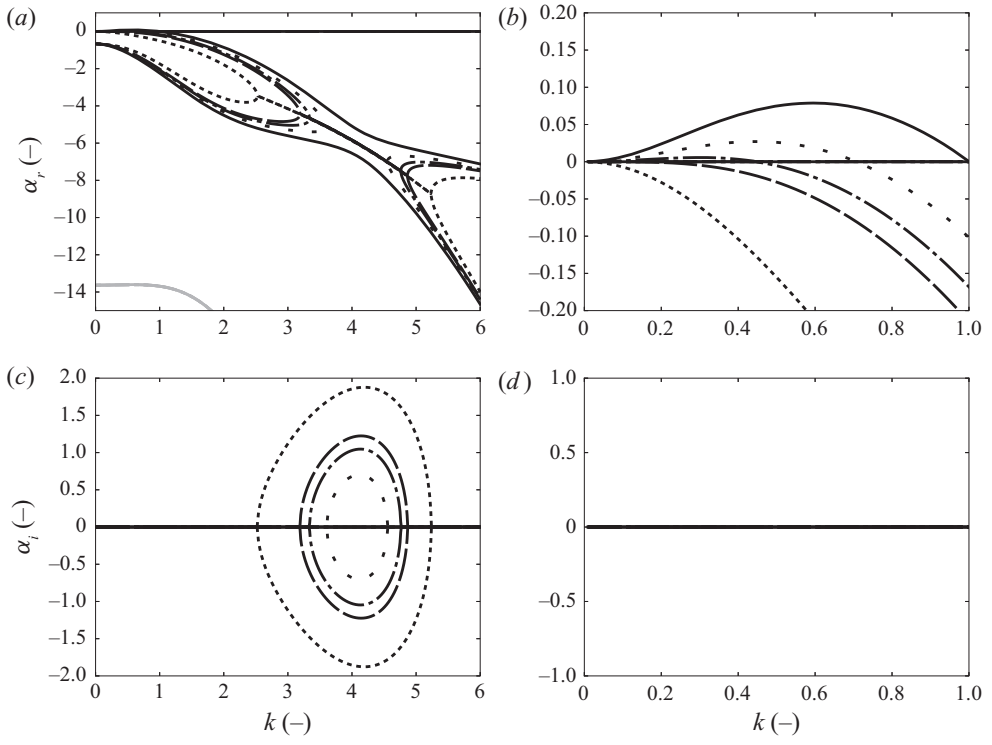

Figure 14. Solutions of the dispersion relation in an azimuthal magnetic field for $Oh = 0.55$, $\mu_r = 2$, $\delta_w = 0.1$ and different Γ_m; Panels (b,d) are (a,b) α_r as a function of k, (c,d) α_i as a function of k. Panels (b,d) are blow-ups of (a,c); —— $\Gamma_m = 0$; - - - $\Gamma_m = 0.5$; —-- $\Gamma_m = 0.8$; —— $\Gamma_m = 1$; - - - - - - - - $\Gamma_m = 2$. Black lines correspond to the capillary solutions and grey lines to the hydrodynamic solutions.

a solenoid replacing R_s by r. Thus, the range of z, where the infinite length hypothesis is valid to within 1 %, can be found in figure 12, while ensuring that the wire radius is included in the radial distance r. The same conclusions as for the solenoid can be drawn replacing Λ_s by $\Lambda_w + d/L_w$, with d the distance to the wire. However, this is less restrictive for the wire because $\Lambda_w + d/L_w$ is much smaller than the ratio Λ_s. For example, the experiment of Arkhipenko *et al.* (1981) used a cylindrical conductor as a wire with radius $R_w = 1$ mm and two lengths $L_{w1} = 180$ and $L_{w2} = 500$ mm (table 1). These values give $\Lambda_{w1} = 5.6 \times 10^{-3}$ and $\Lambda_{w2} = 2.0 \times 10^{-3}$. The distance to the wire, corresponding to the presence of ferrofluid, increases from $d = 1.1$ to $d = 1.8$ mm. Referring to figure 12, it emerges in this experiment that the infinite length hypothesis of the wire is valid for 85 % of the wire in the most unfavourable case ($L_{w1} = 180$ and $d = 1.8$ mm) and 96 % in the most favourable case ($L_{w2} = 500$ and $d = 1.1$ mm). For the experiment of Bourdin *et al.* (2010), this hypothesis is valid for 92 % of the wire by taking the values $\Lambda_w = 3.0 \times 10^{-3}$, $L_w = 500$, and $d = 2.3$ mm.

A comparison with the experiments on ferrofluid cylinders of Arkhipenko *et al.* (1981) and Bourdin *et al.* (2010) is presented in figures 16 and 17, respectively. We saw that in these experiments the infinite length hypothesis is valid for at least 85 % of the wire. It is therefore relevant to compare them with the present theory. Figure 16 shows that the consideration of ferrofluid viscosity does not greatly influence the wavelength $\Lambda^* = 1/k^*$ of the most unstable mode compared to the inviscid theory. Nevertheless, it improves the prediction of the growth rate of this mode. The difference with the experimental

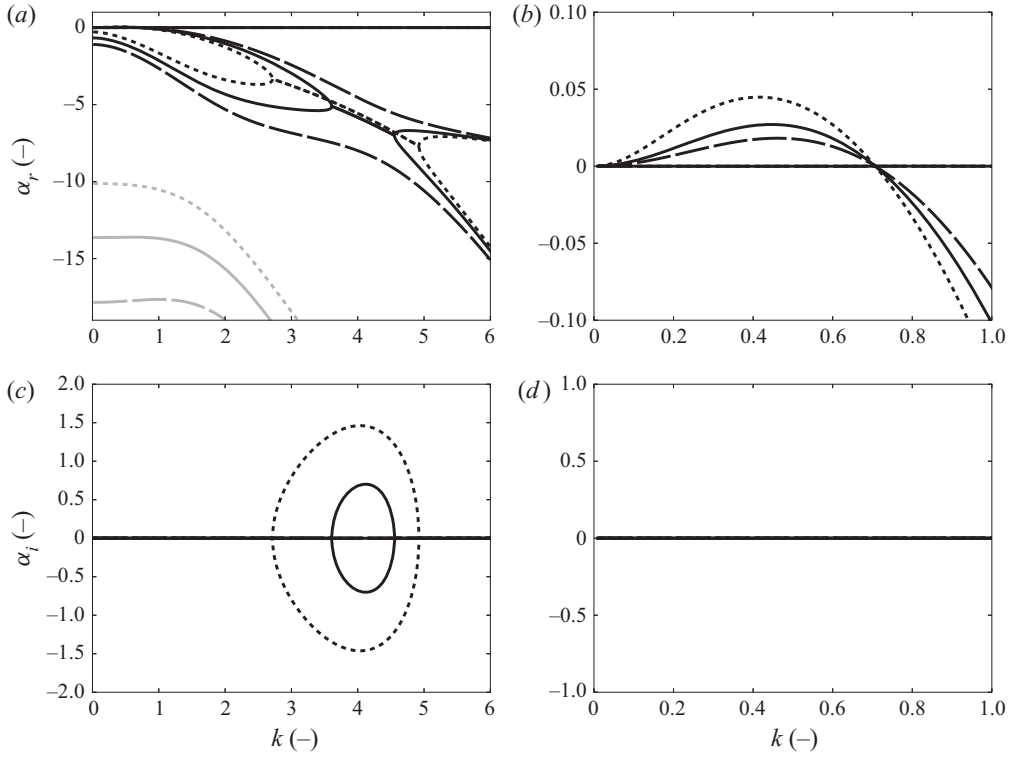

Figure 15. Solutions of the dispersion relation in an azimuthal magnetic field for $Oh = 0.55$, $\mu_r = 2$, $\Gamma_m = 0.5$ and different δ_w; (*a*,*b*) α_r as a function of k, (*c*,*d*) α_i as a function of k. Panels (*b*,*d*) are blow-ups of (*a*,*c*); - - - - - - - - $\delta_w = 0.01$; —— $\delta_w = 0.1$; — — $\delta_w = 0.2$. Black lines correspond to the capillary solutions and grey lines to the hydrodynamic solutions.

data probably relates to the fact that in the experiment, the surrounding fluid does not have a negligible viscosity or density. Figure 17, which compares the present theory to the experimental data of Bourdin *et al.* (2010) using the quantity $\alpha^2/(N_{Bo,m} - 1 + k^2)$, shows that the consideration of ferrofluid viscosity reduces the discrepancy between the experiment and theory. Only the case of $N_{Bo,m} = 6.51$ is plotted here. All the curves are overlapped for the different values of $N_{Bo,m}$.

4.3. *Destabilising magnetic field*

For this final case, an inverse approach is used. Instead of imposing a shape on the magnetic field, we searched for the shape to destabilise the ferrofluid cylinder compared to the case without a magnetic field. We thus searched for a case in which the cutoff wavenumber exceeds 1. We saw previously that axial magnetic fields cannot destabilise the ferrofluid cylinder. So, the dispersion relation (3.33), which considers a solid cylindrical structure, has to be used with expression (3.38) for P_{mag}. Equation (3.39), for the cutoff wavenumber, can be written in a more convenient form to identify the magnetic field shape coefficients

$$\left(\mu_r - \frac{\mu_r\,(\mu_r - 1)\,A_w K_1(k_c) k_c}{\mu_r A_w K_0(k_c) + B_w K_1(k_c)}\right) A^2 + B^2 + \frac{(\mu_r - 1)\,B_w K_0(k_c) k_c}{\mu_r A_w K_0(k_c) + B_w K_1(k_c)} C^2 = \frac{1 - k_c^2}{N_{Bo,m}}. \tag{4.9}$$

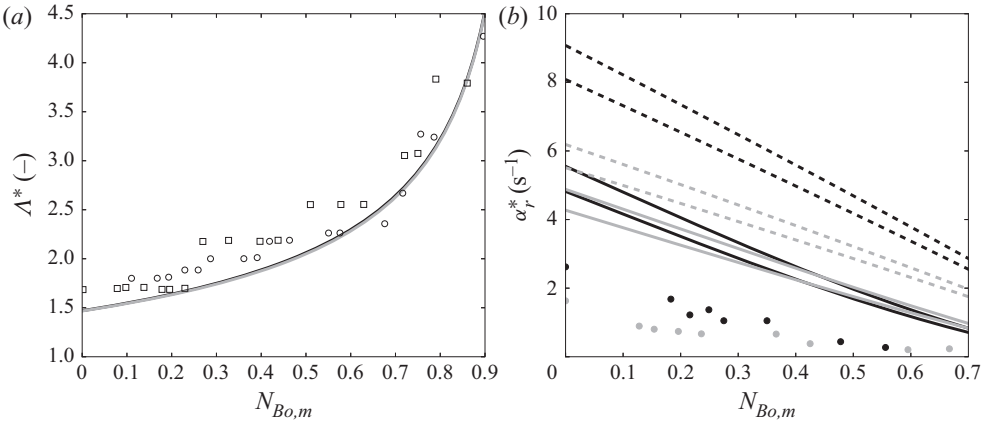

Figure 16. Comparison with the experimental data of Arkhipenko *et al.* (1981) in an azimuthal magnetic field. (*a*) Value of Λ^* as a function of $N_{Bo,m}$; □, experimental data with a column of 18 cm; ◯, experimental data with a column of 50 cm; grey line corresponds to the inviscid theory of Arkhipenko *et al.* (1981) and black line to the present viscous theory. (*b*) Value of α_r^* as a function of $N_{Bo,m}$; dots correspond to the experimental data; dashed lines to the inviscid theory of Arkhipenko *et al.* (1981) and solid lines to the present viscous theory. Black corresponds to $R_0 = 2.1$ mm and grey to $R_0 = 2.8$ mm. Identical lines are plotted for the ferrofluids FF1 and FF2 of table 2.

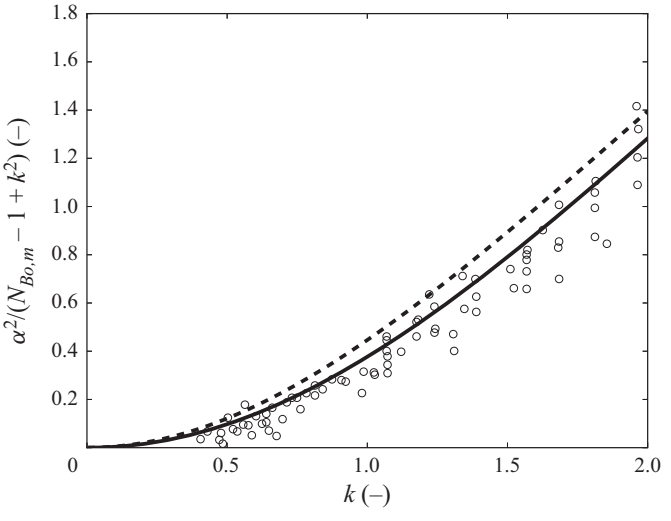

Figure 17. Comparison with the experimental data of Bourdin *et al.* (2010) in an azimuthal magnetic field. Circles correspond to experimental data for different $N_{Bo,m}$ from 1.85 to 11.57, the dashed line to the inviscid theoretical prediction made in Bourdin *et al.* (2010) and the solid line to the present viscous theory plotted for the ferrofluid FF3 of table 2 and $N_{Bo,m} = 6.51$.

A cutoff wavenumber greater than 1 is sought for this case. The right-hand side of (4.9) must therefore be negative. Because A, B and C are the magnetic field components, they are not complex, and A^2, B^2 and C^2 are positive. Furthermore, the coefficient before C^2 is always positive for $\delta_w < 1$. Therefore, only the coefficient before A^2 can be negative. This means that, to have a cutoff wavenumber greater than 1, a magnetic field with a radial component is necessary. It confirms the result that a magnetic field normal to a free surface is destabilising (Melcher 1963; Rosensweig 1985). However, the coefficient before

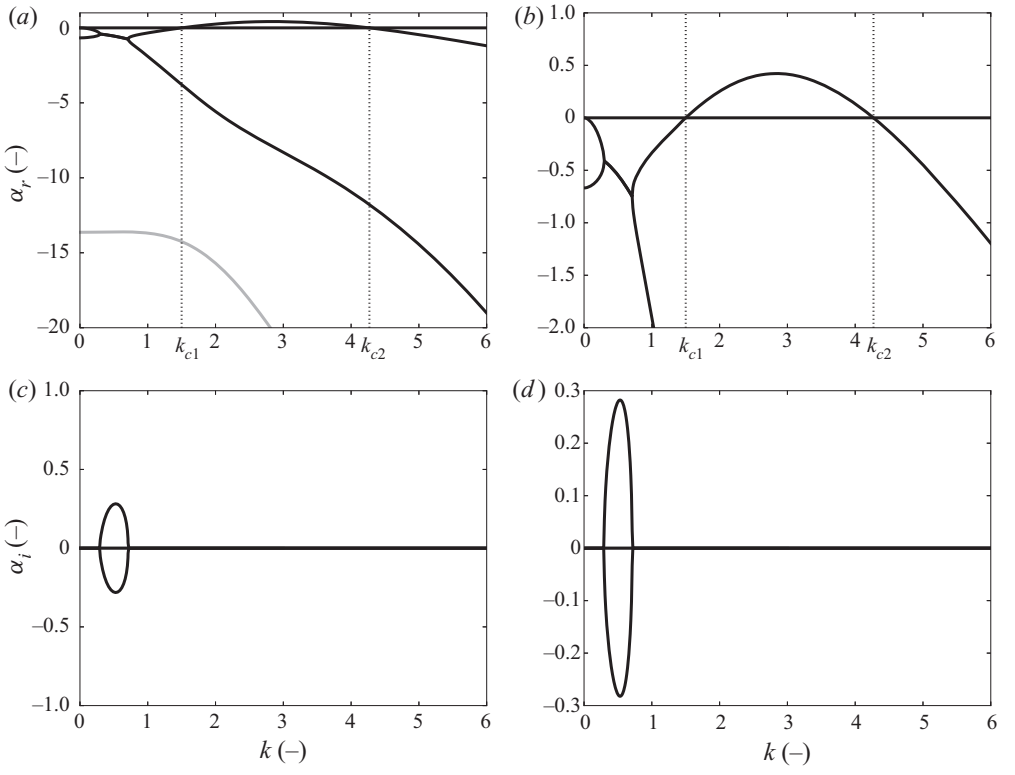

Figure 18. Solutions of the dispersion relation in a radial destabilising magnetic field for $Oh = 0.55$, $\mu_r = 5$, $\Gamma_m = 0.425$ and $\delta_w = 0.1$; (*a*,*b*) α_r as a function of k, (*c*,*d*) α_i as a function of k. Panels (*b*,*d*) are blow-ups of (*a*,*c*). Black lines correspond to the capillary solutions and the grey line to the hydrodynamic solution. Vertical dotted lines represent the values of k_{c1} and k_{c2}.

A^2 is not always negative, and for a given μ_r and δ_w, there is a condition on the possible cutoff wavenumbers. By taking the values $\mu_r = 2$ and $\delta_w = 0.1$, the coefficient before A^2 is negative only for $k_c > 2.95$. With $\mu_r = 5$ and $\delta_w = 0.1$, the condition becomes $k_c > 1.275$. In the following, these latter values are chosen.

To determine the components of the destabilising magnetic field, the value of k_c should be imposed to verify the condition given by the values of μ_r and δ_w. If a value $k_c = 1.5$ is wanted for $\mu_r = 5$ and $\delta_w = 0.1$, (4.9) becomes

$$-0.735296A^2 + B^2 + 1.21732C^2 = \frac{-1.25}{N_{Bo,m}}. \tag{4.10}$$

From relation (4.10), we can see that an infinite number of magnetic fields can destabilise the ferrofluid cylinder. One possibility is the pure radial magnetic field $\{1/r, 0, 0\}$, which leads to $N_{Bo,m} = 1.7$ (so $\Gamma_m = 0.425$).

In figure 18, the capillary and first hydrodynamic solutions are represented for the purely radial magnetic field case with $Oh = 0.55$, $\mu_r = 5$, $\delta_w = 0.1$ and $\Gamma_m = 0.425$. One specificity characterises this case compared to the previous ones; the unstable regime is no longer found at the small k values between 0 and k_c but rather at intermediate values of k between two cutoff wavenumbers k_{c1} and k_{c2}. As expected, $k_{c1} = 1.5$, while $k_{c2} \simeq 4.27$. For $k < k_{c1}$ and $k > k_{c2}$, the regime is stable with the oscillation part between $k_1 = 0.29$ and $k_2 = 0.71$. Furthermore, the values of α at $k = 0$ for the capillary solutions (including

https://doi.org/10.1017/jfm.2021.171 Published online by Cambridge University Press

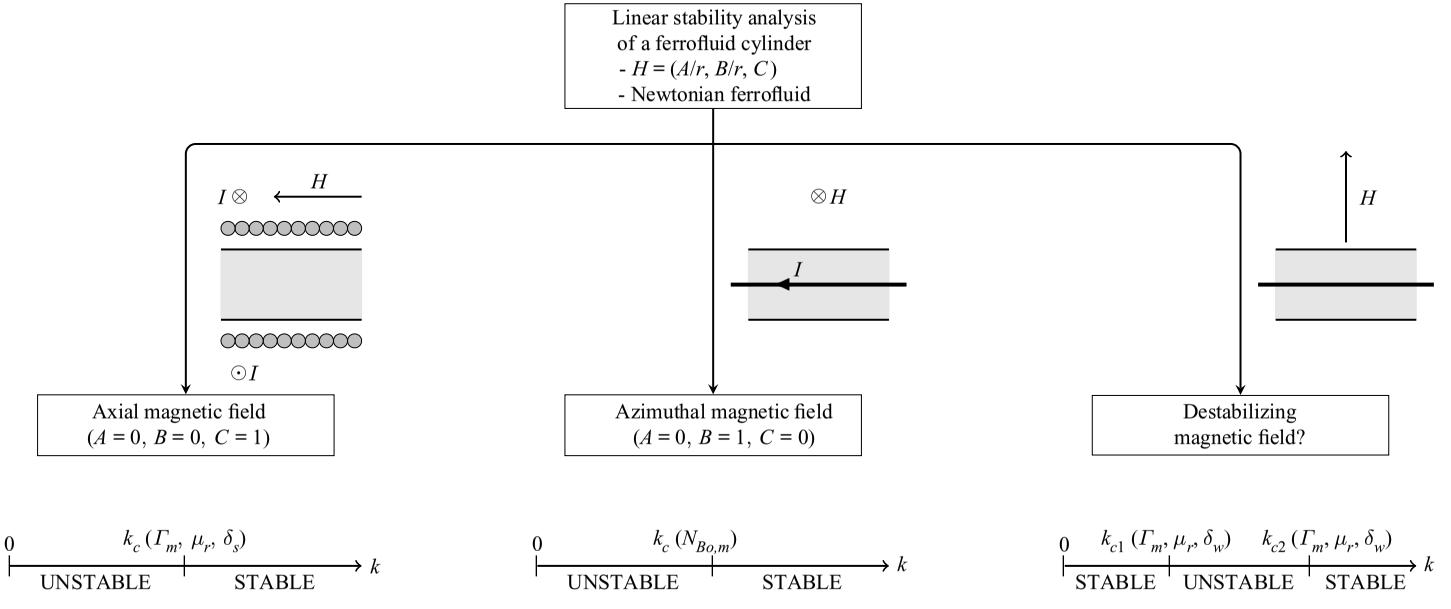

Figure 19. Summary diagram of the results.

the trivial $\alpha = 0$ solution) and the hydrodynamic solution are the same as those for the azimuthal magnetic field case with $\delta_w = 0.1$, which shows that these values depend on the radius of the solid structure rather than μ_r or the magnetic field shape.

This case shows that it is theoretically possible to increase wavenumber values with an unstable ferrofluid cylinder, although it is unknown whether this is experimentally achievable.

5. Conclusion

We performed a linear stability analysis of a ferrofluid cylinder under a steady magnetic field of general shape. The admissible shapes of the magnetic field were found in the form $(A/r, B/r, C)$ with three constants (A, B, C). We considered the viscosity of the ferrofluid by assuming the Newtonian behaviour of the ferrofluid. A small-amplitude axisymmetric disturbance was imposed on the basic state. We linearised the dimensionless equations and obtained dispersion relations for axial and non-axial magnetic field shapes. These relations depend on four dimensionless parameters: dimensionless wavenumber k, Ohnesorge number Oh, relative magnetic permeability μ_r and magnetic parameter Γ_m. For non-axial shapes, a fifth parameter appears: dimensionless wire radius δ_w owing to the presence of wire to prevent singularity at $r = 0$. We formulated, for each shape, an equation for the cutoff wavenumber delimiting the stable/unstable regime and a condition for the total stability of the ferrofluid cylinder. Different shapes for the magnetic field were studied. The first was an axial magnetic field $(A = 0, B = 0, C = 1)$ in which the ferrofluid cylinder becomes increasingly stable as the magnetic field intensity, through Γ_m, or μ_r increases. We also examined the influence of the solenoid, commonly used in prior experiments to create this magnetic field, showing that its effect is negligible for a high solenoid radius. However, the required radius increases rapidly for high magnetic field intensity. The solenoid should also be long enough to consider a homogeneous magnetic field. For the axial magnetic field case, a link was made between the temporal and spatial analyses of the ferrofluid liquid jet to determine from which jet velocity an infinite ferrofluid cylinder can represent jet behaviour. For a high magnetic field intensity, a lower velocity is needed. The second case was an azimuthal magnetic field $(A = 0, B = 1, C = 0)$ in which wire was used to prevent singularity at $r = 0$. In this case, the ferrofluid cylinder can be stabilised for all wavenumbers from a specific magnetic field intensity. Our theory that takes into account ferrofluid viscosity better explains the experimental results compared to the existing theories without ferrofluid viscosity. Finally, a case that destabilises the ferrofluid cylinder was found. A magnetic field with a radial component is necessary for this purpose, and the radial magnetic field shape $(A = 1, B = 0, C = 0)$ is such an example. The particularity observed here is that the unstable regime no longer concerns small wavenumbers but intermediate wavenumbers. This behaviour could allow us to control the drop size created during a ferrofluid jet breakup. The main results of this work are summarised in figure 19. Future studies should consider the nonlinearities due to the advection term in the momentum balance equation and the magnetic contributions in order to predict satellite drops, which are undesirable in printing applications with magnetic inks for example. Other effects could also be studied such as the influence of the surrounding fluid viscosity. Indeed, when ferrofluids are used in medicine, they must be injected in a viscous biological liquid.

Acknowledgements. The authors would like to thank Professor I. Mutabazi for initiating this interlaboratory project and contributing to useful discussions on its two parts.

Funding. This work was supported by LabEx EMC3 through the INFEMA (INstabilities of FErrofluid flows in MAgnetic fields) project, commonly conducted by LOMC (Normandie Univ, UNIHAVRE, CNRS) and CORIA laboratories.

Declaration of interests. The authors report no conflict of interest.

Author ORCIDs.
Marie-Charlotte Renoult https://orcid.org/0000-0003-0613-0888.

References

Abdel Fattah, A.R., Ghosh, S. & Puri, I.K. 2016 Printing microstructures in a polymer matrix using a ferrofluid droplet. *J. Magn. Magn. Mater.* **401**, 1054–1059.

Ahmed, A., Qureshi, A.J., Fleck, B.A. & Waghmare, P.R. 2018 Effects of magnetic field on the spreading dynamics of an impinging ferrofluid droplet. *J. Colloid Interface Sci.* **532**, 309–320.

Alexiou, C., Tietze, R., Schreiber, E., Jurgons, R., Richter, H., Trahms, L., Rahn, H., Odenbach, S. & Lyer, S. 2011 Cancer therapy with drug loaded magnetic nanoparticles – magnetic drug targeting. *J. Magn. Magn. Mater.* **323** (10), 1404–1407.

Arkhipenko, V.I., Barkov, Y..D., Bashtovoi, V.G. & Krakov, M.S. 1981 Investigation into the stability of a stationary cylindrical column of magnetizable liquid. *Fluid Dyn.* **15** (4), 477–481.

Bashtovoi, V.G. & Krakov, M.S. 1978 Stability of an axisymmetric jet of magnetizable fluid. *J. Appl. Mech. Tech. Phys.* **19** (4), 541–545.

Blyth, M.G. & Părău, E.I. 2014 Solitary waves on a ferrofluid jet. *J. Fluid Mech.* **750**, 401–420.

Bourdin, E., Bacri, J.-C. & Falcon, E. 2010 Observation of axisymmetric solitary waves on the surface of a ferrofluid. *Phys. Rev. Lett.* **104** (9), 094502.

Brenn, G. 2017 *Analytical Solutions for Transport Processes: Fluid Mechanics, Heat and Mass Transfer*, 1st edn. Mathematical Engineering. Springer.

Callaghan, E.E. & Maslen, S.H. 1960 The magnetic field of a finite solenoid. *NASA Tech. Note* NASA-TN-D-465.

Chandrasekhar, S. 1961 *Hydrodynamic and Hydromagnetic Stability*. International Series of Monographs on Physics. Clarendon.

Charles, S.W. 1987 Some applications of magnetic fluids – use as an ink and in microwave systems. *J. Magn. Magn. Mater.* **65** (2), 350–358.

Charles, S.W. & Popplewell, J. 1982 Properties and applications of magnetic liquids. *Endeavour* **6** (4), 153–161.

Doak, A. & Vanden-Broeck, J.-M. 2019 Travelling wave solutions on an axisymmetric ferrofluid jet. *J. Fluid Mech.* **865**, 414–439.

Fabian, M., Burda, P., Šviková, M. & Huňady, R. 2017 The influence of magnetic field on the separation of droplets from ferrofluid jet. *J. Magn. Magn. Mater.* **431**, 196–200.

Favakeh, A., Bijarchi, M.A. & Shafii, M.B. 2020 Ferrofluid droplet formation from a nozzle using alternating magnetic field with different magnetic coil positions. *J. Magn. Magn. Mater.* **498**, 166134.

García, F.J. & González, H. 2008 Normal-mode linear analysis and initial conditions of capillary jets. *J. Fluid Mech.* **602**, 81–117.

Guerrero, J., González, H. & García, F.J. 2012 Spatial modes of capillary jets, with application to surface stimulation. *J. Fluid Mech.* **702**, 354–377.

Jackson, J.D. 1962 *Classical Electrodynamics*. Wiley.

Keller, J.B., Rubinow, S.I. & Tu, Y.O. 1973 Spatial instability of a jet. *Phys. Fluids* **16** (12), 2052.

Luck, R., Zdaniuk, G.J. & Cho, H. 2015 An efficient method to find solutions for transcendental equations with several roots. *Intl J. Engng Maths* **2015**, 1–4.

Löwa, N., Fabert, J.-M., Gutkelch, D., Paysen, H., Kosch, O. & Wiekhorst, F. 2019 3D-printing of novel magnetic composites based on magnetic nanoparticles and photopolymers. *J. Magn. Magn. Mater.* **469**, 456–460.

Lübbe, A.S., *et al.* 1996 Clinical experiences with magnetic drug targeting: a phase I study with 4′-epidoxorubicin in 14 patients with advanced solid tumors. *Cancer Res.* **56** (20), 4686–4693.

Melcher, J.R. 1963 *Field-coupled Surface Waves: A Comparative Study of Surface-coupled Electrohydrodynamic and Magnetohydrodynamic Systems*. MIT Press.

Nguyen, N.-T. 2012 Micro-magnetofluidics: interactions between magnetism and fluid flow on the microscale. *Microfluid Nanofluid* **12** (1–4), 1–16.

PANKHURST, Q.A., CONNOLLY, J., JONES, S.K. & DOBSON, J. 2003 Applications of magnetic nanoparticles in biomedicine. *J. Phys.* D*: Appl. Phys.* **36** (13), R167–R181.

PULFER, S.K., CICCOTTO, S.L. & GALLO, J.M. 1999 Distribution of small magnetic particles in brain tumor-bearing rats. *J. Neurooncol.* **41** (2), 99–105.

PÉREZ, J.-P., CARLES, R., FLECKINGER, R. & LAGOUTE, C. 2009 *Electromagnétisme: fondements et applications : avec 300 exercices et problèmes résolus*. OCLC: 1029110105.

RADWAN, A.E. 1988 Effect of magnetic fields on the capillary instability of an annular liquid jet. *J. Magn. Magn. Mater.* **72** (2), 219–232.

RADWAN, A.E. 1990*a* Capillary instability of a streaming cylindrical liquid jet submerged in a streaming fluid under the influence of magnetic fields. *J. Magn. Magn. Mater.* **86**, 184–196.

RADWAN, A.E. 1990*b* Effect of magnetic fields on the capillary instability of an annular liquid jet having a solid mantle. *J. Magn. Magn. Mater.* **84** (1), 189–200.

RAJ, K. & BOULTON, R.J. 1987 Ferrofluids – properties and applications. *Mater. Des.* **8** (4), 233–236.

RAJ, K., MOSKOWITZ, B. & CASCIARI, R. 1995 Advances in ferrofluid technology. *J. Magn. Magn. Mater.* **149** (1), 174–180.

RAJ, K. & MOSKOWITZ, R. 1990 Commercial applications of ferrofluids. *J. Magn. Magn. Mater.* **85** (1), 233–245.

RANNACHER, D. & ENGEL, A. 2006 Cylindrical Korteweg–de Vries solitons on a ferrofluid surface. *New J. Phys.* **8** (6), 108–108.

RENOULT, M.-C., BRENN, G., PLOHL, G. & MUTABAZI, I. 2018 Weakly nonlinear instability of a Newtonian liquid jet. *J. Fluid Mech.* **856**, 169–201.

ROSENSWEIG, R.E. 1985 *Ferrohydrodynamics*. Cambridge Monographs on Mechanics and Applied Mathematics. Cambridge University Press.

SCHERER, C. & FIGUEIREDO NETO, A.M. 2005 Ferrofluids: properties and applications. *Braz. J. Phys.* **35** (3a), 718–727.

SHLIOMIS, M.I. 1974 Magnetic fluids. *Sov. Phys. Uspekhi* **17** (2), 153–169.

SMYTHE, W.R. 1950 *Static and Dynamic Electricity*. International Series in Pure and Applied Physics. McGraw-Hill 201, 306–309.

SUDO, S., IKOHAGI, T., NISHIYAMA, H. & KATAGIRI, K. 1999 Dynamic behavior of a magnetic fluid jet injected from a vibrating nozzle. *J. Magn. Magn. Mater.* **201**, 306–309.

SUDO, S. & ISE, K. 2004 Droplet production from a capillary jet of magnetic fluid under a magnetic field. *Intl J. Appl. Electrom.* **19** (1–4), 169–174.

SUDO, S., WAKUDA, H. & ASANO, D. 2010 Capillary jet production of magnetic fluid by electromagnetic vibration. *Intl J. Appl. Electrom.* **33** (1–2), 63–69.

TAKTAROV, N.G. 1975 Disintegration of streams of magnetic fluid. *Magnetohydrodynamics* **11** (2), 156–158.

WEINSTEIN, M. 1988 The effect of a vertical magnetic field on the capillary instability of a liquid–liquid jet. *J. Franklin Inst.* **325** (4), 537–543.

YAKUBENKO, P.A. & SHUGAI, G.A. 1996 Absolute, convective, and global instability of a magnetic liquid jet. *Fluid Dyn. Res.* **18** (6), 325–335.

YARIN, A.L. 1993 *Free Liquid Jets and Films: Hydrodynamics and Rheology*. Interaction of Mechanics and Mathematics Series. Longman Scientific & Technical.

ZAKINYAN, A. 2017 Instability of a magnetic fluid jet in a transverse magnetic field. *Chem. Engng Commun.* **204** (4), 434–439.